Design and Experimental Analysis of a Large Scale Natural Convection Test Loop

A Thesis
Presented in Partial Fulfillment of the Requirements for the
Degree of Master of Science
with a
Major in Nuclear Engineering
in the
College of Graduate Studies
University of Idaho
by
James Richards

Major Professor: Richard Christensen, Ph.D.
Committee Members: David Arcilesi, Ph.D.; Michael McKellar, Ph.D.
Department Administrator: Richard Christensen, Ph.D.

August 2020

Authorization to Submit Thesis

This thesis of James Richards, submitted for the degree of Master of Science with a Major in Nuclear Engineering and titled "Design and Experimental Analysis of a Large Scale Natural Convection Test Loop," has been reviewed in final form. Permission, as indicated by the signatures and dates below, is now granted to submit final copies to the College of Graduate Studies for approval.

Major Professor:	Richard Christensen, Ph.D.	Date
Committee Members:	David Arcilesi, Ph.D.	Date
	Michael McKellar, Ph.D.	Date
Department Administrator:	Richard Christensen, Ph.D.	Date

Abstract

This thesis presents the design, development, and preliminary testing for a natural circulation test loop at the University of Idaho. The loop stands 19-ft tall, and is designed to handle high temperatures and pressures. To use the loop, a heater and heat exchanger were developed to add and remove heat at the same rate. A 4 kW immersion heater adds heat, and a custom tube-in-tube heat exchanger removes heat. A pressurizer and control system was also designed for higher pressure tests. A pump, valve, and flow meter combination were used to the flow of cooling water, and thus the heat removed.

Temperature profiles were analyzed for low pressure tests (48 kPa, 7psi) and high pressure tests (1724 kPa, 250 psi). Heat exchanger temperature profiles were also measured and heat exchanger effectiveness determined. Results show reasonable agreement with CFD results from other studies. Suggestions for improving the loop are also given.

Acknowledgments

I would like to personally thank Dr. Richard Christensen, who helped provide technical expertise, management insights, and research funding for the project. I would also like to thank Larry Zirker and Jesse Webb, whose fabrication expertise was invaluable in this project. Additionally, I would like to give thanks to Dr. Amin Mirkouei, Dr. Lee Ostrom, and Dr. Michael McKellar, who all provided feedback and insight that led to a safe and efficient laboratory environment. Lastly, I would like to thank my committee member, Dr. Mckellar and Dr. David Arcilesi for providing pertinent and meaningful feedback through the writing process.

Dedication

Dedicated to Cori, because she's alright.

Table of Contents

List of Tables

List of Figures

Chapter 1: Introduction

Natural circulation is a phenomena in which fluid flow is driven via thermal gradients and without the use of pumps or other turbomachinery. To induce natural circulation, fluid is heated to a point that its buoyancy force overcomes gravity and frictional losses to move upward. The lower density fluid flows until overcome by gravitational and/or friction, or until heat is removed via a heat sink. When heat is removed, the fluid flows downward. In a closed loop, the downward flow returns the cold fluid to the heat source, starting the cycle again. This process effectively transfers heat from the hot end to the heat sink without any need for pumps or forced convection.

1.1 Natural Circulation in Nuclear Engineering

The nuclear industry has been investigating natural circulation for years, but that interest dramatically increased after the 2011 incident at the Fukushima Daiichi nuclear plant. A large earthquake caused the reactors to shutdown and rely on diesel backup generators for core cooling pumps. An ensuing tsunami destroyed the backup generators and, with no way to remove the reactors' decay heat, three of six reactors suffered partial meltdowns and at least two hydrogen explosions occurred. The Fukushima incident marked the worst nuclear accident since Chernobyl.

After the Fukushima meltdowns, the nuclear industry sought designs that would minimize the vulnerabilities exposed by the earthquake and tsunami in Japan. Passive safety systems, or safety systems that do not require personnel or equipment to work, became a point of focus.

Natural circulation as a passive safety measure became a larger area of research in the nuclear industry. By using the reactor as a heat source and the outside of the core as a heat sink, a core with a coolant could remove heat indefinitely. This would eliminate the need for the backup generators that were so vulnerable in the Fukushima incident. Companies started to incorporate natural circulation cooling in their water reactor designs and the U.S. Regulatory Commission (NRC) has certified a design without backup cooling pumps because natural circulation was shown to sufficiently cool the reactor. Advanced reactor design and research has also turned towards natural circulation, seeking to quantify molten salt and liquid metal natural convection phenomenon.

1.2 Purpose and Overview

This thesis puts forth development of an apparatus for natural convection flow testing, compare results to computer models for validation purposes, and suggest improvements to system design and testing strategies. The experimental apparatus has been built to drive natural convection flow through a piping system. The system is pressurized to achieve higher water temperatures without boiling. Models are used to help design the experimental loop control scheme and compare data to other working fluids.

The subsequent chapters give background, experimental methods and apparatus design, and results of natural circulation tests. Chapter 2 discusses natural circulation and pressurizer theory, existing testing and data collection systems, working fluid scaling, and other background material. Chapter 3 puts forth the loop design methodology, in which equipment sizing, heat exchanger design, pressurizer design, and system control are discussed. The experimental results are presented and analyzed in Chapter 4.

The final section, Chapter 5, gives conclusions and uses this experiment to inform recommendations for improvement.

Chapter 2: Theory and Background

A static fluid balances the upward buoyant force against resisting viscous and gravitational forces. To instigate flow, the buoyant forces must overcome downward forces to move the fluid upward. Natural convection, or natural circulation, is when a heat source or temperature gradient increase the buoyant force to a point that it overcomes downward forces and drives flow upward. Natural convection does not utilize turbo-machinery to instigate flow.

2.1 Fluid Flow Background

To understand natural circulation, it is important to first understand the forces that act on fluid and cause or inhibit flow. Consider a control volume of a fluid, such as the one shown in Figure 2.1. This control volume is governed by the three conservation laws: conservation of mass, conservation of energy and conservation of momentum.

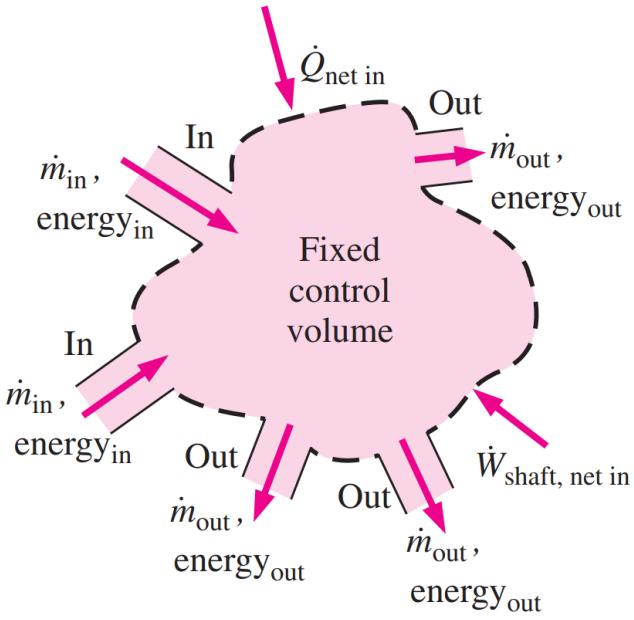

Figure 2.1: A sample control volume with multiple inlets and outlets [1].

The conservation of mass for a control volume of fluid states that the change in fluid over a given time is equal to the fluid entering the control volume minus the fluid leaving the control volume. In a fixed pipe, mass is conserved because mass flow rate of fluid entering the pipe is equal to mass flow rate of fluid leaving the pipe. This phenomenon is given mathematically in Equation 2.1.

$$\frac{dm_{cv}}{dt} = \dot{m_{in}} - \dot{m_{out}} \tag{2.1}$$

Derivation of natural convection governing equations requires an energy balance. The most basic form

of an energy balance is given in Equation 2.2. $\dot{E_{in}}$ and $\dot{E_{out}}$ represent the total flow of energy in and out, respectively. In a transient system, the energy accumulates or dissipates within the control volume. In a steady state system, the rate of energy added to the control volume is equal to the rate of energy removed from the control volume.

$$\frac{dE_{cv}}{dt} = \dot{E_{in}} - \dot{E_{out}} \tag{2.2}$$

The energy balance can expanded by incorporating all the energy inputs, outputs, and accumulation in a given control volume. This robust approximation is given in Equation 2.3.

$$\dot{Q_{net,in}} + \dot{W_{net,in}} = \frac{d}{dt}\int_{CV} e\rho dV + \sum_{in} \dot{m}(\frac{P}{\rho} + u + \frac{V^2}{2} + gz) - \sum_{out} \dot{m}(\frac{P}{\rho} + u + \frac{V^2}{2} + gz) \tag{2.3}$$

Where $\dot{Q_{net,in}}$ is the net heat added into the system, $\dot{W_{net,in}}$ is the net shaft work into the system, $\frac{d}{dt}\int_{CV} e\rho dV$ is the accumulation of energy, and $\sum_{in} \dot{m}(\frac{P}{\rho} + u + \frac{V^2}{2} + gz) - \sum_{out} \dot{m}(\frac{P}{\rho} + u + \frac{V^2}{2} + gz)$ is the difference in energy in and out due to flow work (P/ρ), internal energy (u), kinetic energy $(V^2/2)$, and potential energy (gz).

Momentum is also conserved in a control volume undergoing natural circulation flows. When energy is added to the system, the heat decreases the density of the fluid. When that fluid achieves a large enough density gradient to overcome the gravity, friction, other losses, etc, the fluid is driven upward.

2.2 Natural Circulation in Nuclear Systems

Several reactor designs are leveraging natural circulation for reactor core cooling or passive safety features in accident scenarios. The Nuscale SMR design eliminates primary side pumps in lieu of a naturally circulating system [2]. Molten salt reactors and liquid metal reactors rely on natural circulation in pools to achieve even core heating [3]. The Molten Salt Nuclear Battery (MsNB), a microreactor under development, relies on natural circulation as the only means of inducing primary side flow [4].

In addition to passive cooling during operation, several reactor designs employ natural circulation during off-normal situations. The GE PRISM reactor, a fast spectrum, liquid metal reactor, employs the Reactor Vessel Auxiliary Cooling System (RVACS) [5]. The RVACS system transfers heat from the core to the containment via radiation. The containment unit is then air cooled via naturally circulating air being heated and moving away upward, away from the containment. GE anticipates that this would be able to cool the PRISM reactor indefinitely. The AP-1000, a gigawatt scale pressurized water reactor developed by Westinghouse, utilizes a passive system for 7 days of emergency cooling. As temperature or pressure increase in various parts of the system, actuators trip allowing core make up water to flow via natural circulation to the core. This is designed to keep the core cooled during a loss of coolant accident (LOCA) [6]. The Chinese National Nuclear Corporation HPR-1000 operates in a similar manner, holding a tank of water at the upper end of containment that will fall in a LOCA and then circulate around the containment, allowing heat to pass through heat exchangers to the secondary side [7]. The Advanced European Pressurized Reactor (EPR) developed by Areva is a boiling water reactor that employs a similar

system to passively cool itself in emergency scenarios. In a meltdown, the corium, or melted fuel bundle material is allowed to collect at the bottom of the core while the bottom of the containment is flooded, creating an interface where heat can be transferred from the core into the water [8]. Figure 2.2 shows this design.

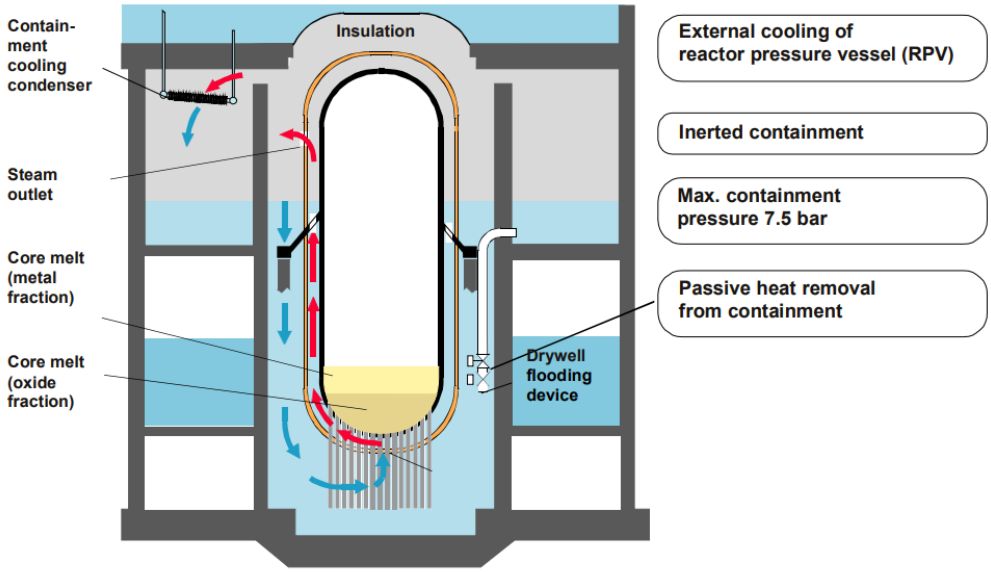

Figure 2.2: EPR emergency passive cooling system. Naturally circulating water removes heat from the core and ejects it to the condenser [8].

In addition to circulating fluid in normal operation and emergency scenarios, another use for natural circulation in nuclear power come via heat pipes. Heat pipes are pipes that move heat from one side of the pipe to the other via internal natural circulation and mass flow processes. Figure 2.3 illustrates how heat pipes work. One end of the pipe is heated and the walls transfer heat into a working fluid on the inside of the pipe. The internal fluid has a density gradient along the length of the pipe. This density gradient, as well as some mass transfer mechanics, such as an internal wick, allow fluid to move to the cold end of the pipe [9]. This end can then input heat into a working fluid or surrounding space. Heat pipes for reactor cooling are popular in microreactor [4, 10] and space reactor [11] designs.

2.3 Experimental Testing Methods for Natural Convection

Experimental testing for natural convection phenomena generally depend of the working fluid and the desired flow conditions. Closed loop testing apparatuses, such as thermosiphons, are good for liquids. Apparatuses that are open to the atmosphere via chimneys are usually used for gas convection testing.

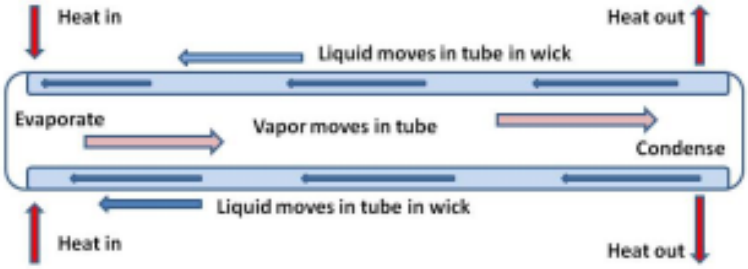

Figure 2.3: Heat pipe schematic. The heat is added to one side of the system, evaporating the internal working fluid. The fluid travels to the cold end via natural convection and capillary action up the wick. Some heat pipes do not contain wicks and work entirely on natural circulation. Figure from [12].

2.3.1 Thermosiphons

A thermosiphon is an apparatus that comprises of a closed loop, filled with a working fluid that is either in one or two phases. They often contain a heat source at one end and a chiller or heat exchanger to remove heat at the other. Many thermosiphons are vertical in orientation, but some work has been done on natural convection in horizontal thermosiphons or angled orientations [13]. Loops can also be square, rounded, or tordial in shape. Thermosiphons range from bench-top scale to multiple meters tall. A thermosiphon schematic is shown in Figure 2.4.

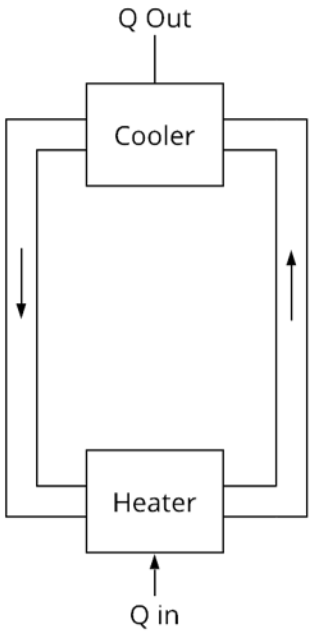

Figure 2.4: Simple thermosiphon schematic featuring lower hot end, upper cold end, directional flow from hot to cold.

Test thermosiphons have helped quantify natural circulation for a large number of use cases, such as solar heating, geothermal applications, or nuclear safety. Solar thermosiphons are used to transfer heat from solar collectors into useful forms for electricity or residential heating. Lower temperature ranges require careful consideration when choosing a working fluid. Esen and Esen utilized refrigerants such as R-134a, R407C, and R410A to boil at the correct temperature, allowing for the transfer of heat more efficiently. In geothermal power, the deep wells can act as thermosiphons, especially using CO_2 plume techniques [14].

Thermosiphons for nuclear research come in different sizes and generally focus on water as a working fluid. The L2 loop, used by the International Atomic energy Agency (IAEA) as a benchmark experimental apparatus, is a 1m high square loop, shown in Figure 2.5.

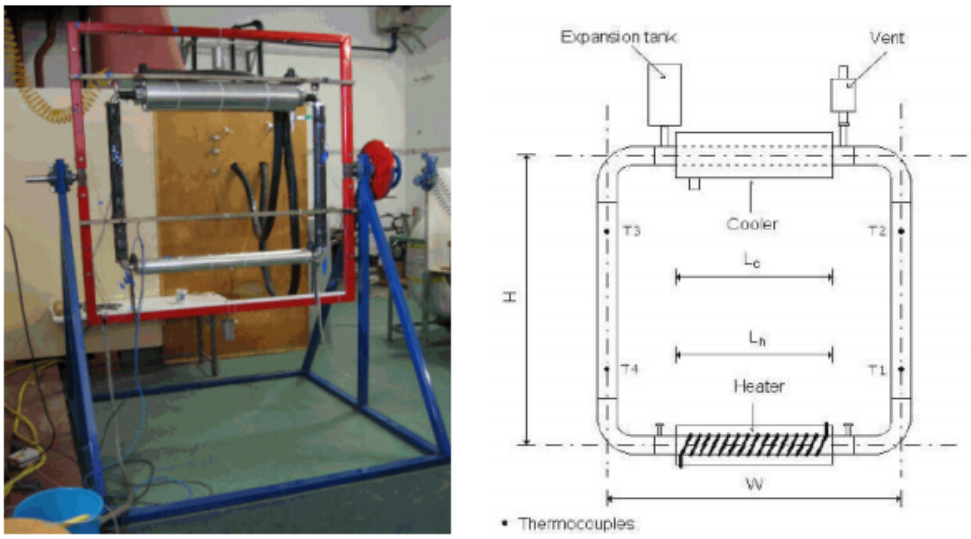

Figure 2.5: L2 thermosiphon and schematic [15].

2.3.2 Other Experimental Apparatuses

While thermosiphons work well for liquid or two phase system, many gas phase natural convection test apparatuses are open to atmosphere. The gaseous working fluid is heated at the bottom and exits at the top, working in a similar manner to a simple residential fireplace or wood stove. These types of experiments are useful because they can simulate air removing heat from a reactor vessel in an incredibly simple configuration. This configuration can also quantify helium circulation characteristics and heat transfer in High Temperature Gas Reactors (HTGR).

One of the largest gaseous natural convection experiments occurs at the Natural Convection Shutdown Heat Removal Test Facility (NSTF) at Argonne National Laboratory (ANL) [16]. The NSTF, shown in 2.6, was designed to test natural convection that would occur in high temperature gas reactors. This equipment differs from a thermosiphon because it is not a closed loop. Rather it has chimneys that change discharge lengths and flow paths. The system is modular because different channel flow paths can

be specified for testing varied geometry. The NSTF system uses fiber optic temperature sensors for high thermal fidelity at high temperatures.

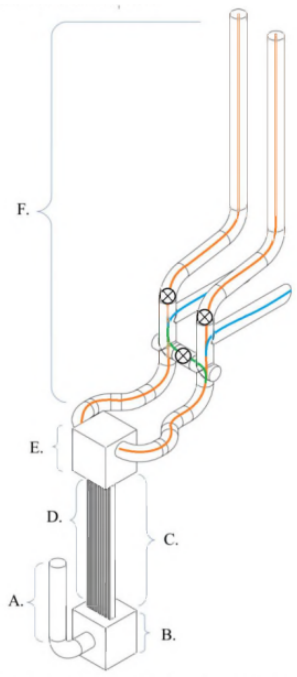

Figure 2.6: Simplified mode of the NSTF Facility. A. inlet downcomer, B. inlet plenum, C. heated cavity, D. risers, E. outlet, F. chimney. The various flow paths are modeled in the different colors, controlled by valves [16].

2.4 Natural Convection Computational Models

Natural convection simulation models offer researchers the ability to design experimental set ups, investigate circulation through complex geometries, or understand flows in extreme conditions. The majority of natural convection modeling utilizes CFD or process modeling tools, while some researchers develop custom codes from first principles models.

2.4.1 Computational Fluid Dynamics

Computational fluid dynamics offers a high fidelity tool for simulating specific fluid behaviour during natural circulation. Alizadehdakhel et al. modeled a two phase thermosiphon, which compared favorably to measured temperature and flow values obtain through experimentation [17]. Ho et al. analyzed the thermosiphon system system in the Cold Neutron Source of the Open Pool Australian Light Water Reactor. Their CFD models suggested that natural convection in the thermosiphon was enough to keep the cold neutron source [18].

High fidelity CFD models, in tandem with particle imaging velocitry (PIV) or other physical visualization method, help further understanding of specific flow patterns. Wang et al. validated a flow patterns in their experimental, two-phase, thermosiphon using CFD. Different boiling regimes were observed in

the physical system and the model predicted these with high accuracy [19]. Similarly, Ghandi et al. matched results of a particle imaging velocitry experiment to their CFD simulations and found that the flow was moving as expected [20, 21].

In addition to thermosiphon behavior, CFD offers insight into natural convection in specific nuclear applications, such as pool type reactors or passive cooling systems. Pal et al. modeled a passive cooling system for use in a light water reactor. They modeled the system under transient conditions in order to quantify startup period conditions [22]. Pialla et al. reviewed several different CFD analyses of a liquid sodium reactor. The natural circulation of liquid sodium in the core was modeled by several different processes [23].

2.4.2 Process Modeling Software

When detailed process information is more important than flow characteristics, process modeling has been used to model systems that require natural circulation. Process modeling is better suited for system wide models, especially those that require equipment such as pumps, heat exchangers, turbines, etc. Several commercially available process modeling software packages fill this need.

One such tool, RELAP5, has been used by extensively by nuclear researchers. Hedayat used RELAP to validate that natural circulation in a pool type reactor would passively cool the core in a shutdown situation or station blackout situation. The analysis modeled points of interest, such as a flapper safety valve, with a higher fidelity. [24]. Freitag modeled a light water SMR, similar to the Nuscale design, and demonstrated that the natural circulation in the primary side would be sufficient for reactor operation [25]. RELAP is also well suited for two phase natural circulation, such as the two phase thermosiphon modeled by Mcduffee et al []. Their analysis modeled the Thermosiphon Test Loop and sought to verify experimental data. Hussain and Nawaz modeled the AP-1000 LOCA sequence in RELAP5, investigating the effect of different mechanical failures on the natural circulation system's ability to cool the core [6]. Additional packages for RELAP, such as the SCADAP package, also extend RELAP's ability to handle transient natural circulation and apply that to nuclear accident scenarios [26].

Other thermosiphon, or natural circulation focused, process models have been developed in Aspen Hysys, Flownex, Aspen Plus, or Modelica. Luzzi et al. developed an object-oriented model written in the Modelica modeling process modeling language [15]. Their model generally agreed with experimental data and was as accurate as analogous CFD models.

2.4.3 Other Modeling Techniques

Custom models have also played a role in the application and understanding of natural circulation. Zaidi developed a support vector regression model that predicted circulation rates in boiler equipment [27]. Zuo and Gunnerson developed a thermosiphon model based on first principles derivations. The model agreed well with experimental results, leading the authors to suggest the first principles approach would be useful in thermosiphon optimization and design [28]. Xu also found that agreement between first principles numerical models and experimental data is sufficient for prediction and design purposes [29]. Cheng et al present a 1-dimensional model of a square thermosiphon with a cooler comprising the top leg and a heater comprising the bottom. The authors found that the 1-dimensional model gives

reasonably accurate results when compared with experimental data [30].

2.5 Natural Convection Scaling in Experiments and Models

Natural convection test loops offer researchers the ability to gather data without building full scale units or using expensive of harmful working fluids through the use of scaling laws. In fluid mechanics, scaling laws are derived from dimensionless parameters to relate flow in one set of conditions to different conditions. For example, Vijayan and Austregesilo found that a natural circulation loop of the same height as PWR flows, and a diamater no smaller than 23.7 mm, could stably predict PWR natural circulation [31]. Basu et al. proposed a non-dimensional model that would work under a wide range of natural convection loops and could be scaled using the Richardson number rather than the Grashoff number that is traditionally used [32].

In addition to scaling water systems, scaling parameters have been shown to predict flows in molten salt systems. Shin et al. found that experimental Dowtherm A flows could be scaled to predict molten salt flows with reasonable accuracy (within 30%) [33]. Oyama et al. use a water convection loop to validate natural convection flows for safety analysis of a sodium fast reactor [34]. Lee et al. took scaling a step further, evaluating the harmony between scaled water tests and liquid metal reactor conditions. They found that, though water and sodium had different Prandlt numbers, they could use the water to predict the liquid metal temperatures after scaling [35].

2.6 Heat Exchanger Design

Many thermosiphons and natural convection experimental apparatuses use heat exchangers to add or remove heat. This section briefly discusses types of heat exchangers and different design strategies.

Heat exchangers move heat from one fluid to another. Generally, this is achieved by moving the hot fluid through an inner tube, or network of tubes, and the cold fluid through an outer shell. The most basic heat exchanger occurs in a concentric pipe, with a single inner tube. Tube in tube exchangers place multiple tubes within a shell with the fluid flowing in a co-current or counter-current manner. More sophisticated designs, such as shell-in-tube heat exchangers, might incorporate cross flow or baffles to increase heat transfer.

Heat exchangers can be quantified using two methods; log-mean temperature difference (LMTD) or number of transfer units (NTU) method. The LMTD method, expressed in Equations 2.4 - 2.7 for a counter current heat exchanger, requires a knowledge of and outlet temperatures. LMTD assumes that the system is single phase, steady state, and that the effects of kinetic and potential energy are negligible.

$$q = UA\Delta T_{lm} \tag{2.4}$$

$$\Delta T_{lm} = \frac{\Delta T_1 - \Delta T_2}{Ln(\Delta T_1) - Ln(\Delta T_2)} \tag{2.5}$$

$$\Delta T_1 = T_{h,i} - T_{c,o} \tag{2.6}$$

$$\Delta T_2 = T_{h,o} - T_{c,i} \tag{2.7}$$

The number of transfer units (NTU) method quantifies the rate of heat transfer. It is often used when there are insufficient temperatures specified for LMTD analysis. The NTU of a heat exchanger is a function of effectiveness and minimum heat capacity ratio. Effectiveness can be found using Equation 2.8.

$$\epsilon = \frac{q}{q_{max}} \tag{2.8}$$

The variable q_{max} is defined as the maximum possible heat transfer rate in an idealized heat exchanger of infinite length. When the idealized heat exchanger transfers all heat possible, the cold outlet and the heat inlet approach the same temperature. The maximum heat transfer is found by Equation 2.9. The minimum heat capacity rate, either C_h for hot or C_c for cold, is used to determine the maximum heat transfer with the difference between the hottest temperature, T_h, i, and coldest, T_c, i.

$$\begin{aligned} C_c < C_h : q_{max} &= C_c(T_{h,i} - T_{c,i}) \\ C_c > C_h : q_{max} &= C_h(T_{h,i} - T_{c,i}) \\ C_h &= \dot{m} c_{p,h} \\ C_c &= \dot{m} c_{p,c} \end{aligned} \tag{2.9}$$

Once any two design variables such as effectiveness, heat capacity ratio (C_c/C_h) or NTU, are known, the unknown design variable can be found using charts such as Figure 2.7. These plots are dependent on geometry and flow direction. The figure shown is for a tube in tube, counter-current heat exchanger.

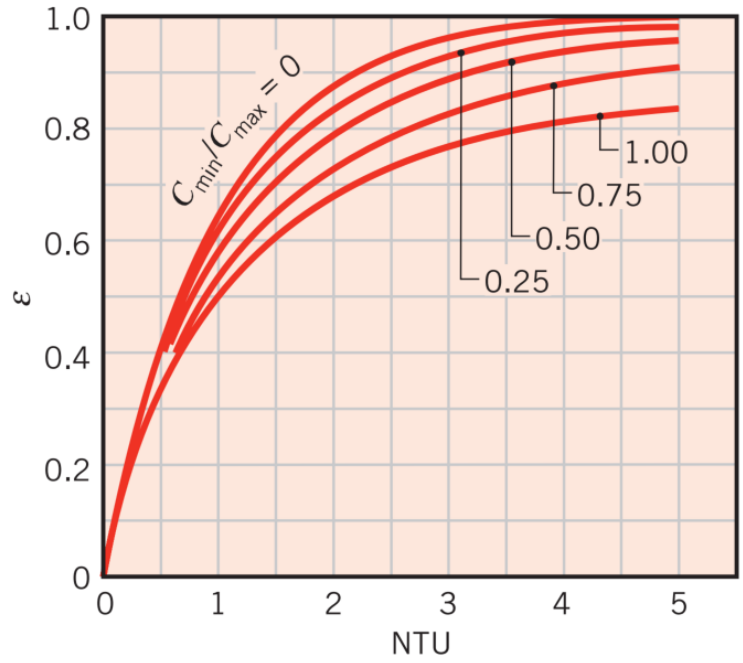

Figure 2.7: NTU effectiveness plot for counter-current flow heat exchangers [36].

Chapter 3: Natural Convection Test Loop Design and Methodology

This chapter discusses the design and implementation of a natural convection loop, or thermosiphon, for testing natural convection phenomena in pressurized water. The required experimental needed to be free-standing, robust enough to withstand moderate to high temperatures and pressures, instrumented to provide meaningful data, fit within laboratory constraints, and have the ability to continue beyond this specific project.

3.1 Operating Conditions

Initially, this system was designed to run using water as a working fluid and at conditions that could be a surrogate for liquid sodium reactor conditions. The desired pressure is 2 MPa (290 psi) since water at this pressure has approximately the same density as liquid sodium at atmospheric pressure [37]. The desired hot side temperature was 200°C (392°F), which would match the density to liquid sodium at reactor outlet conditions of 375°C.

The desired loop operating parameters are shown in Table 3.1. The loop structure was designed to handle higher pressures and temperatures, while parts specific to this project, such as pressure relief valves, were explicitly sized for these experiments.

Table 3.1: Loop Design Conditions

Parameter	Value
Pressure	2 MPa (290 psi)
Hot Temperature	200 °C
Working Fluid	Water

3.2 Physical Design

The loop and supporting rack were originally built under a different research project, meaning adjustments were necessary to add the required equipment and fit the loop correctly in the available lab space. The loop and rack structure, originally 6.1 m (20 ft) tall, needed to be adjusted to meet a laboratory clearance of 5.87m (19 ft, 3 in). The loop, as originally constructed, had flanges for adding testing equipment. Figure 3.1 shows the final drawing of the natural convection loop and rack.

The loop is 316 stainless steel, schedule 80, 2.5" pipe. The flanges, rated at 600#, were welded to the piping pieces. The loop consists of two vertical legs, two return joints, and four connection spools. There are two accessory flanges in each corner for adding equipment. Thread-o-let ports were welded on to various locations for the addition of instrumentation equipment. The loop as various stages in the assembly process is shown in Figure 3.2.

The rack frame is 6" square bar mild steel. A 6 ft by 6ft diamond plate base was welded on and reinforced with 6" bar stock steel. The loop rests on the plate and is secured to the rack via u-bolts to prevent lateral motion. Six-inch lag bolts secure the rack to the laboratory floor.

Figure 3.1: Drawing of natural circulation loop and rack.

In order to reduce the loop height so that it fits in the lab, while also creating room for the necessary heater and heat exchanger, the four connection spools were removed. The return joints and the vertical legs where secured directly to each other at opposite corners. On the other corners, the 90-degree flanges are used to attach bypass pieces. This method increases the usable length of heaters or heat exchangers.

3.2.1 Structural Tests

Structural integrity tests were run using Autodesk Inventor's finite element analysis (FEA) Tools [38]. Appendix B has specific mesh data for each FEA analysis run.

The first test investigated the ability of the rack cross beams and plate to support the weight of the loop. The loop, which weighs approximately 680 kg (1500lbs), sits on the reinforced diamond plate and is secured to the cross members on the rack structure via u-bolts. This test showed no significant deformation in the structure. Figure 3.3 shows the displacement output from the FEA analysis. The safety factor, or ratio of yield stress to working stress is 15. Safety factors over 1 are considered acceptable for structures in consistent environments [39].

The second test performed was a moment analysis to investigate the force necessary to tip the apparatus. The FEA tests fixed the front edge and systematically applied a force perpendicular to the rack towards the fixed edge. This simulated a pushing force towards the heavier end of the apparatus, representing the tipping scenario that requires the least amount of force. As seen in Figure 3.4, the analysis showed minimal displacements on the order of thousandths of an inch. The forces applied at the top of the rack did not yield any movement in the base. Note that the floor and lag bolts are modeled in this analysis.

(a) (b)

(c) (d)

Figure 3.2: a) Lower portion of natural circulation loop during fit-up, b) Loop on rack prior to insulation, c) hot leg with insulation and multipoint thermocouples installed, d) Completed loop with insulation, instrumentation, access stairs, and cooling reservoirs.

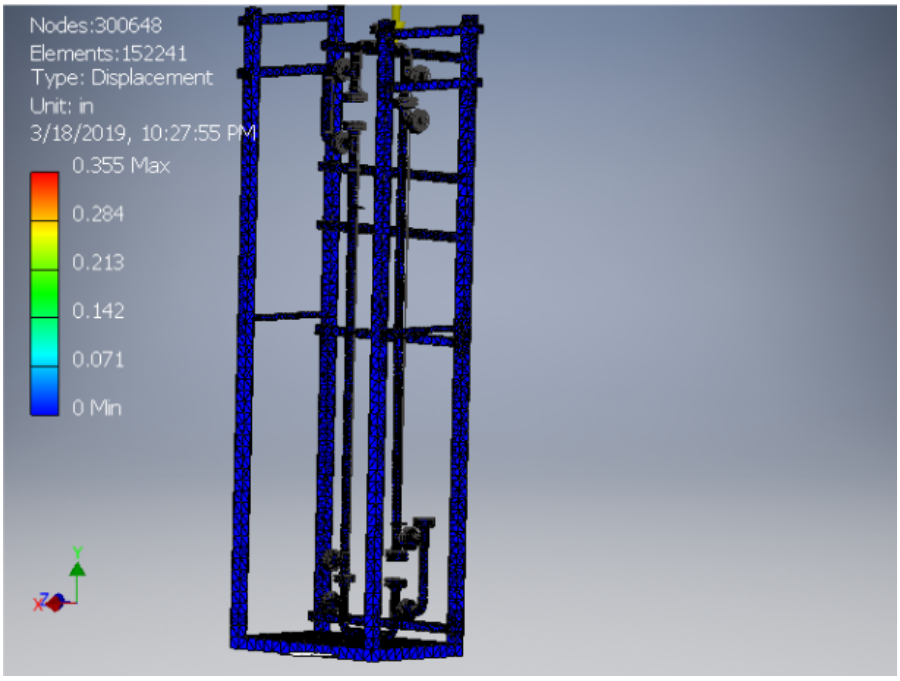

Figure 3.3: Weight and load analysis displacement performed using Autodesk Inventor Finite Element Analysis Package.

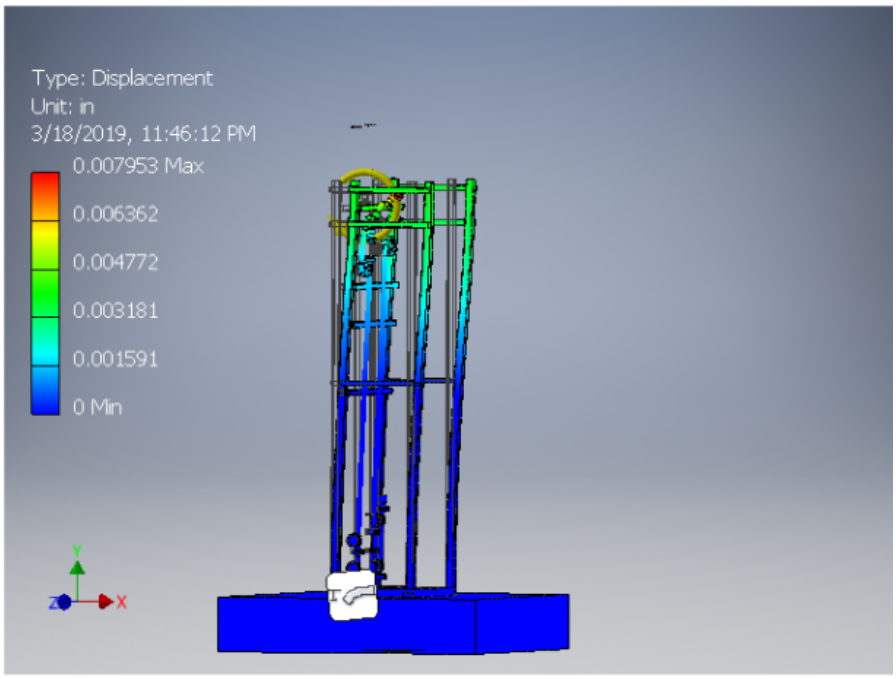

Figure 3.4: Tipping analysis displacement performed using Autodesk Inventor Finite Element Analysis Package.

3.3 Equipment Design

The apparatus, as originally designed, required three pieces of equipment to perform this study; a way to add heat, a way to remove heat, and a way to pressurize the system.

In order to add heat into the system, a jacket was designed to hold an insertion heater in the flow path. The jacket bolts on to accessory flanges, diverting the flow through the jacket. A weld flange was placed at the top of the jacket, and a blind flange was machined to accept the insertion heater threads. The insertion heater was mounted vertically in the jacket. Figure 3.5 shows a drawing of the heater jacket. The height dimension is optimized to allow for the tallest loop that ceiling clearance would allow.

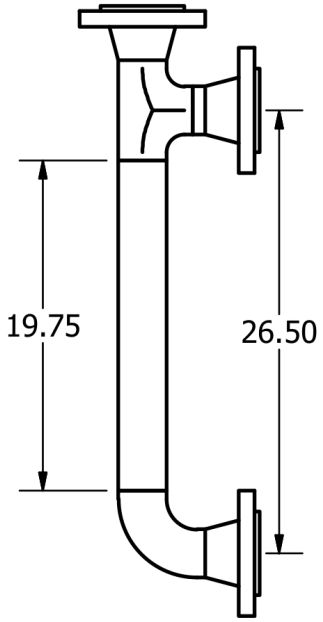

Figure 3.5: CAD drawing for the heater mounding jacket. The heater screws is mounted at top via threaded blind flange. Units in inches.

3.3.1 Heater Sizing

The heat added needs to develop a density gradient large enough that the buoyant force can overcome the pressure losses in the system. This is demonstrated by Equation 3.1. The right side of 3.1 represents the change in head due to differences in density. The left side represents the pressure losses. Change in pressure due to density that is greater than the pressure loss means that the system will flow.

$$\Delta P_l = \Delta \rho g h \tag{3.1}$$

The pressure losses are approximated by the Darcy-Weisbach equation, given in Equation 3.2:

$$\Delta P_l = (f_d \frac{L}{D} + \sum K_L) \frac{\rho \nu^2}{2} \tag{3.2}$$

where P_l is pressure drop, f_d is the Darcy friction factor, L equals vertical length of the flow loop, D is pipe diameter, K_l represents minor loss coefficients, ρ is the density of the fluid, and v is the average velocity of the system. It is important to note that the k_l coefficients used for the expansion and contraction in flow at the heat exchanger contribute a large portion of the pressure drop. Flow moves from a 2.323-in diameter pipe into 8 quarter inch tubes and back out to the larger pipe, incurring a large pressure drop in the process.

For the purposes of this calculation, the Reynolds number, and thus the velocity, acts as the dependent variable and the pressure drop acts as the independent variable.

$$(f_d \frac{L}{D} + \sum K_L) \frac{\rho_{ave} \nu^2}{2} = (\rho_c - \rho_h) g h \tag{3.3}$$

where $\rho_{ave} = \frac{\rho_c + \rho_h}{2}$. Substituting the Reynolds number for velocity in Equation 3.3 yields Equation 3.4.

$$(f_d \frac{L}{D} + \sum K_L) \frac{2Re^2 \mu^2}{h(\rho_c + \rho_h)} = (\rho_c - \rho_h) g \tag{3.4}$$

By varying the Reynolds number in Equation 3.5, and holding the hot side conditions constant at 2 MPa and 200°C, the cold side density can be calculated. The Darcy-Weisbach friction factor of $64/Re$ was used because the majority of the flows analyzed occur within the laminar regime [40]

The temperature that corresponds to cold side density was found using NIST RefProp data for water [41].

$$Q = m c_p \Delta T \tag{3.5}$$

The loop heater was sized to drive natural circulation in water pressurized to 2 MPa. From Figure 3.6, the heater should to provide up to 4000 W to drive flow up through the transitional flow regime. Table 3.2 shows the calculated densities, flow rates, and pressure drops.

Table 3.2: Pressure Drop, Density and Temperature Change for 2 MPa and 200°C Conditions

RE	V(m/s)	$\Delta P_{l,fric}$ (Pa)	$\Delta P_{l,minor}(Pa)$	$\Delta P_{l,hx}$(Pa)	ΔP_l(Pa)	$\rho_{cold}(kg/m^3)$	ΔT(°C)
100	2.64e-04	2.29e-04	4.68e-04	0.06	6.15e-02	865.2	31.4
1000	2.64e-03	2.29e-02	4.68e-02	0.79	8.58e-01	865.3	31.4
2000	5.28e-03	9.17e-02	1.87e-01	1.98	2.26	865.5	31.6
3000	7.92e-03	2.06e-01	4.21e-01	3.57	4.20	865.9	32.0
4000	1.06e-02	3.67e-01	7.48e-01	5.56	6.68	866.4	32.5

A Wattlow 4000 W insertion heater with an 18.75-inch insertion length and a 14.75 heater length was chosen to satisfy the heating and space requirements.

An Aspen HYSYS model was developed to verify the first principles heater sizing calculations [42]. Aspen HYSYS is a commercial process modeling software for thermal and chemical process development.

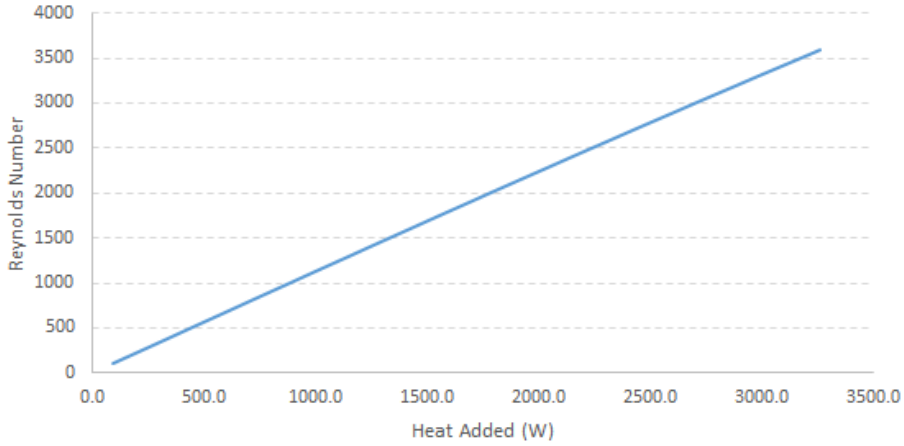

Figure 3.6: Heat required to achieve various working fluid Reynolds numbers.

The thermosiphon was modeled in Hysys using the same conditions as the first principles model. A 2% pressure drop was assumed over the heater and cooling heat exchanger components. Figure 3.7 shows that the Hysys model and the first principles model agree well; within 2%. The HYSYS simulation and the calculations do deviate at higher heat inputs, possible due to the Hysys assumptions on pressure drops.

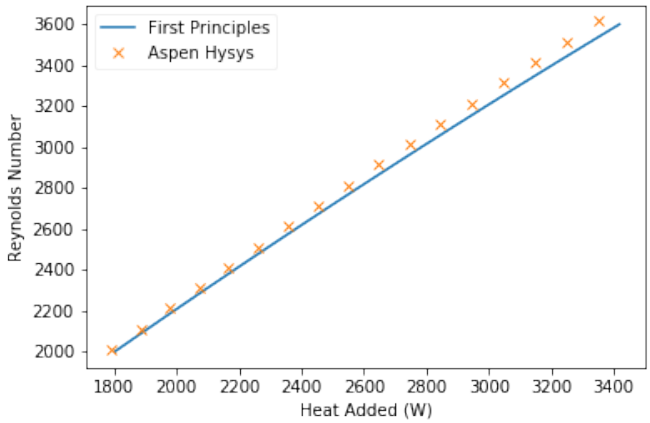

Figure 3.7: HYSYS model comparison to first principles model. Models agree within 2% over the entire scale.

The heater input varies using a 0 to 240V Variac transformer. The Variac is adjusted to the desired voltage via manual control. The Table 3.3 below displays the heat output for a given voltage. A variable transformer was used, rather than a temperature controller or thermostat, because the natural convection loop requires a consistent heat input rather than a consistent temperature.

With the heater sized, it was also necessary to design a heat removal system at the opposite end of

Table 3.3: Variac Voltage and Corresponding Heat Input From Main Loop Heater

Variac Voltage	Heater Input
40 V	667 W
80 V	1333 W
120 V	2000 W
160 V	2667 W
200 V	3333 W
240 V	4000 W

the apparatus. A tube in tube heat exchanger design was investigated. The exchanger would bolt on to upper accessory flanges, allowing the internal cooling water to move through a tube bank. Outside of the bundle of tubes, but inside a jacket, cooling water flows in a counter-current to remove heat.

This heat exchanger needed to meet size and heat removal design parameters. The heated length of the tube bundle needed to remain under 0.48m (19") so that the apparatus would have appropriate ceiling clearance. The heat exchanger also needed the ability to remove all the heat that the heater can input into the system (4 kW).

With the heat exchanger duty known, approximate hot side temperatures and flow rates that were calculated in the previous analysis, and the geometry requirements accounted for; the heat exchanger was designed to remove heat at the same rate the heater inputs heat. The exchanger was optimized for the best heat transfer with the fewest number of tubes and a length that would meet ceiling clearance. Through the log-mean temperature difference method and Equation 3.5, it was found that eight 1/4" tubes meet the heat transfer and size requirements. The tubes used in the exchanger were copper in order to achieve better heat transfer in a smaller space. The coefficient of expansion between 316 stainless steel is 16.0°C^{-1} and copper nickel alloy is 16.2 °C^{-1} [43]. The coefficients of linear expansion differ by less than 2%, so they were deemed reasonable for this application because of the tubes' small size and temperature distribution.

The jacket was built with the same 2.5" nominal pipe as the rest of the system. The tube bundle was welded into place inside the pipe, and ports were inserted for cooling water entrance and exit. Elbows and weld flanges attached the heat exchanger to the accessory ports on the upper end of the system. A drawing of the heat exchanger is shown in Figure 3.8 and the heat exchanger during the build is shown in Figure 3.9.

The cooling water system consists of two 100-gallon reservoirs; one 100-gallon tank and two connected 55 gallon drums, as shown in Figure 3.10. A submersible pump is placed in the cold reservoir. Water is pumped up and through the heat exchanger and down into the second reservoir.

The heat removed is controlled by a flow meter and valve combination. The flow rate is modulated to remove an amount of heat that matches the heater input. Figure 3.12 demonstrates the relationship between cold side flow rate and the amount of heat removed from the loop. Figure 3.13 shows the valve and flow meter combination mounted at the upper end of the loop to control cooling water flow. Figure 3.11 shows the relation between Reynolds number and temperature change from the cold to the hot side.

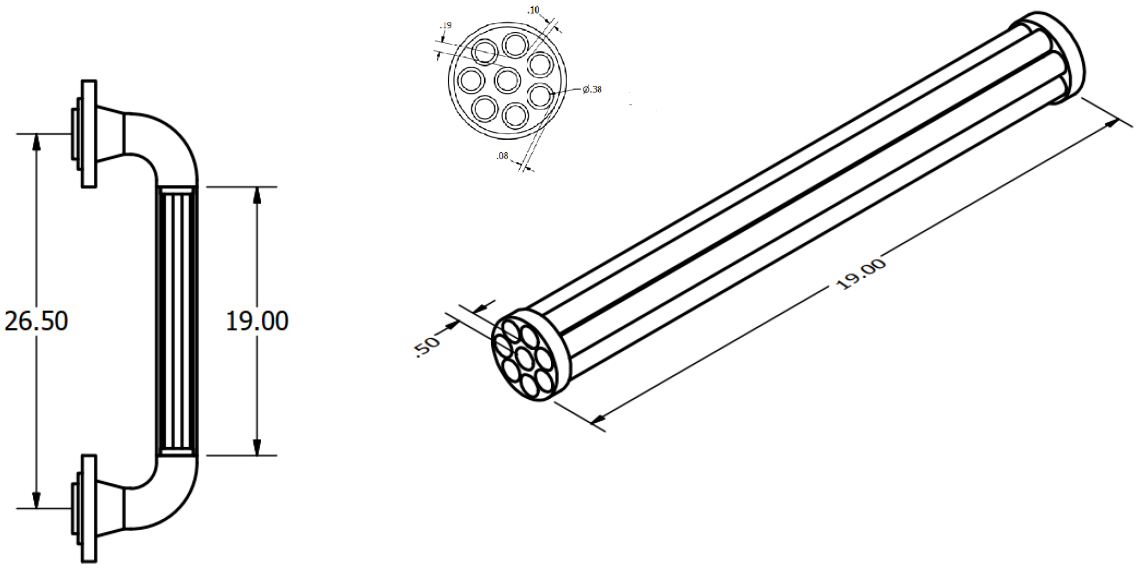

Figure 3.8: Drawing of the heat exchanger, tube bundle, and bundle plate.

Figure 3.9: Jacket, tube, and bundle plate pieces of heat exchanger prior to welding.

Figure 3.10: Cooling water reservoirs.

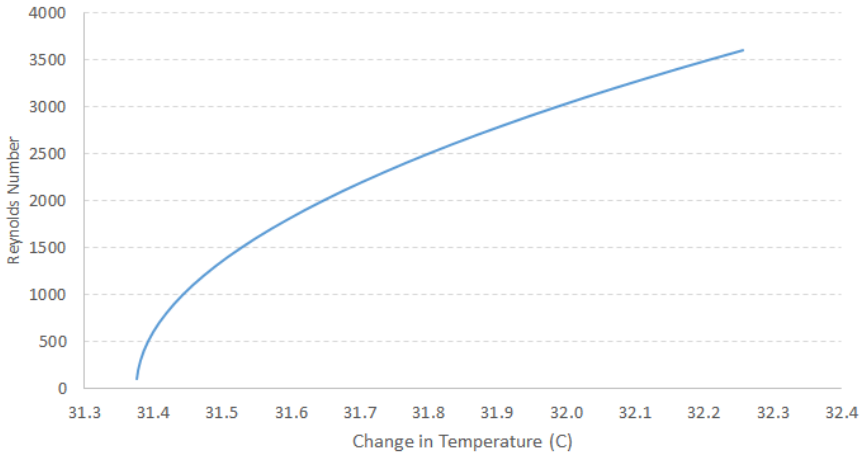

Figure 3.11: Relationship between the Reynolds Number of water in the loop and the temperature change from hot leg to cold leg.

The third piece of equipment that was designed and fabricated specifically for this project was a pressurizer. Because the goal of this investigation was to study single-phase natural convection at higher temperatures, the system needed to be pressurized. The pressurizer built for this analysis acts in a similar manner to LWR pressurizers. An 800 kW heater is placed at the bottom of the pressurizer to boil water. The tube is only connected to the loop at one end, via one of the lower accessory flanges, so as water boils, it rises to the top of the tube and collects. The specific design parameters are presented in Section 4.3 with adjustments that need to be made to the initial design for further testing. Figure 3.14 shows the pressurizer design.

A Tempco TPC-1000 PID temperature controller is used to maintain the temperature in the pressurizer. A thermocouple reads the temperature and the controller adjusts the heater output to maintain the temperature at the saturation point. To monitor level control, sight glass portholes were added to the

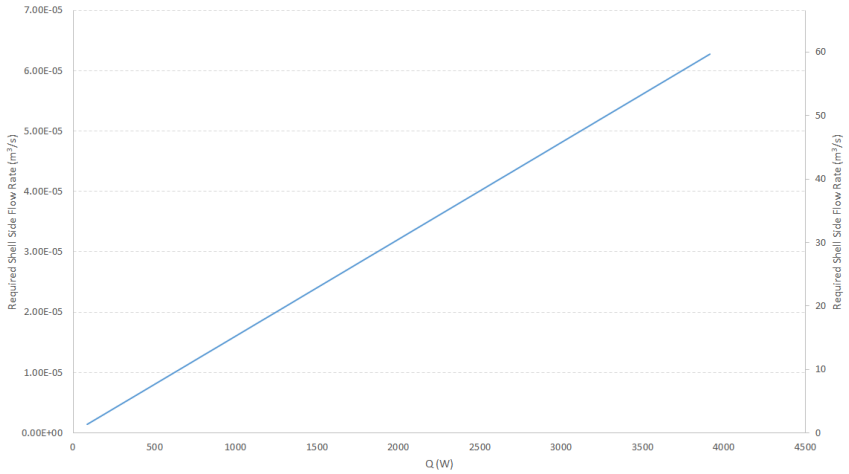

Figure 3.12: Amount of heat removed by heat exchanger plotted against the cooling water flow rate.

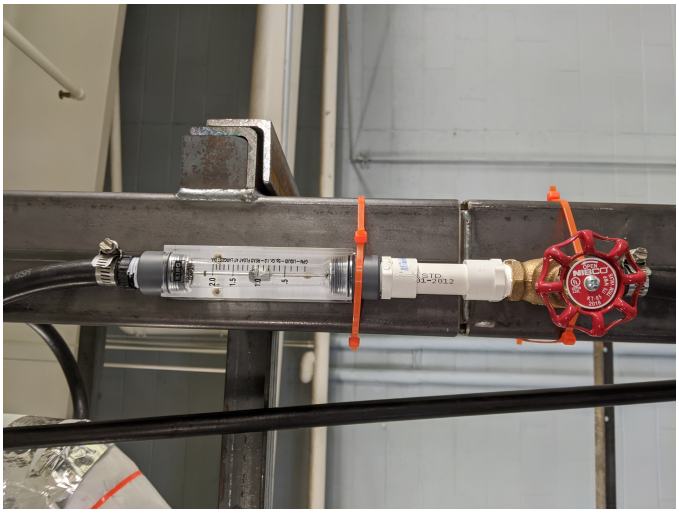

Figure 3.13: Cooling water flow meter and valve.

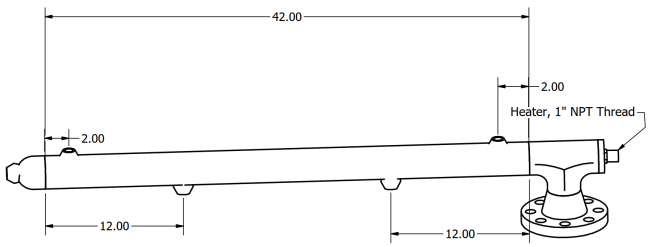

Figure 3.14: Pressurizer design. Note the pressurizer is mounted vertically on the system.

pressurizer so a user would be able to view the level within the system. In large scale pressurizers, level control is generally more of an issue, but the small amounts of heat and fluid used in this pressurizer mean that there is little fluctuation in level, so a manual viewing window is appropriate. For finer control, a level sensor and a multiple-input multiple-output (MIMO) dual PID control scheme could be utilized.

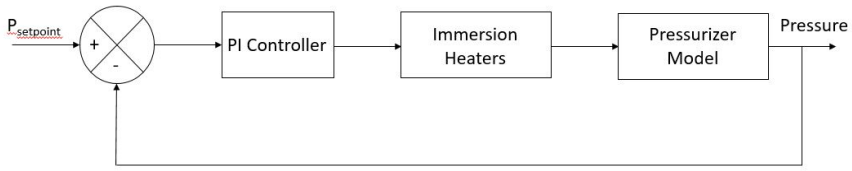

Figure 3.15: Pressurizer control schematic.

The pressurizer differs from PWR pressurizers because there is no cooling water injection nozzle. Instead, the pressurizer is not insulated. Water is allowed to condense and that condensate serves to reduce pressure in the system. This makes the pressurizer, and control scheme, much simpler. The drawback of this method is that it requires a larger heater to overcome the condensation effects when the pressurizer is maintaining or increasing system pressure.

3.4 Instrumentation Design

Temperature, pressure, and flow rate data were recorded during system operation. To measure temperature 6 single point and 4 multipoint thermococuples, built by Idaho Labs crop, are used. The pressure is measured by three Omega pressure transducers and manually by a pressure gauge. The flow is measured ultrasonically via an Omega FDT-21 flow meter. Instrumentation equipment was placed strategically at various points around the loop. The system instrumentation is illustrated in Figure 3.16.

The type K thermocouples, built by Idaho Labs corp, are inserted into the system via a thread-o-let connections that are welded onto the loop at various locations. The single junction thermocouples were inserted so the tip is at the middle of the flow path. The multipoint TCs, which contain 5 measurement points within each rod, are inserted so the first measurement point is just off of the wall. The four multipoint TCs are placed on the hot leg so that the cross sectional temperature profile of the hot flow could be captured. Other TCs are placed in the pressurizer, at the hot entrance and exit of the heat exchanger, in the heater jacket, and at the top and bottom of the loop. The thermocouples were calibrated under the NIST ITS-90 calibration procedure [44] and carry an error of plus or minus 2.2°C.

The pressure transducers were mounted to the loop via impulse lines. The temperature of the working fluid was too high for inline pressure measurement devices. Thus, impulse lines were used to allow the fluid time to cool before entering the PT. The impulse lines were 4' in length and curled to make a compact system. The water flows through the impulse line and stagnates at the PT end, allowing for a pressure measurement at a lower temperature. The PTs were factor calibrated and provided with a voltage curve that was input into the data collection software.

An Omega FDT-21 ultrasonic flow meter was used to make non-invasive flow rate measurements.

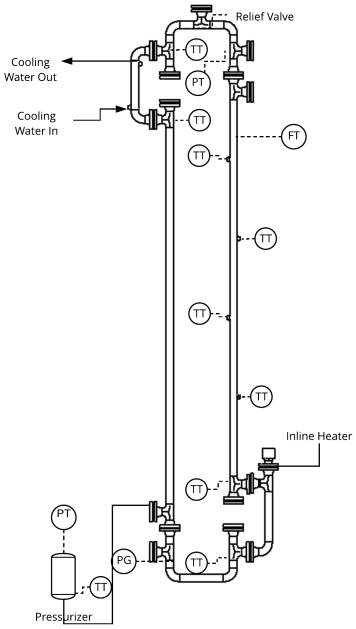

Figure 3.16: Loop control and monitoring schematic. FT represents the flow meter, PT the pressure transducers, TT the thermocouples, and PG the pressure gauge.

The probes are placed on the outside of the pipe and the measurement is sent back and converted to a handheld unit. The flow meter was placed on the upper end of the hot leg.

The majority of data is collected via a National Instruments (NI) Data Acquisition (DAQ) system. Each thermocouple and pressure transducer are connected to the DAQ. The DAQ communicates with a laptop running the LabView software with a custom built front end. Labview collected the data into a central spreadsheet. The flow measurements were saved into the flow meter and transferred to a computer after testing. Figure 3.17 shows the setup for the whole loops monitoring and control system.

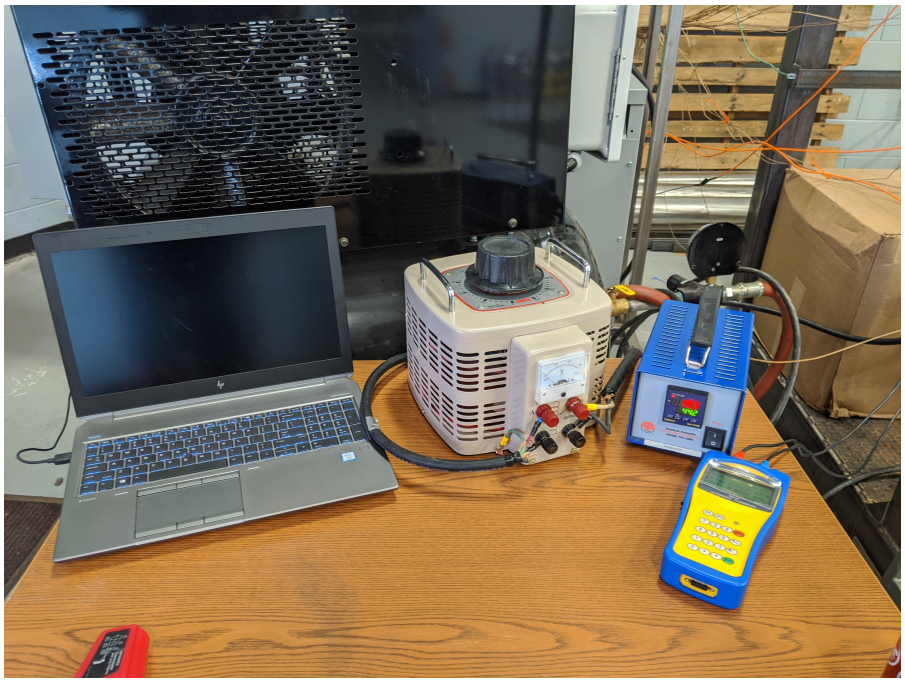

Figure 3.17: Loop control and monitoring system. From left to right: laptop for monitoring temperature and pressure through LabView, variac for controlling main heater input, TEMPCO tpc-1000 temperature controller for pressurizer heater control, OMEGA FDT-21 ultrasonic flowmeter.

Chapter 4: Results of Natural Circulation Flow Experiments

This chapter details the natural convection testing that was completed using this loop. Several changes were made to testing conditions in order to provide rapid meaningful results. The experimental temperatures were run at 50°C, rather than 200°C, because the system had difficulty circulation the heat to reach higher temperatures. Initial experimentation used the static pump to actuate pressure, rather than the pressurizer. Testing focused on validating the heat exchanger's effectiveness and demonstrating natural convection flows.

4.1 Natural Circulation Results

Several days of testing were performed, during which, the main heater voltage and cooling water flow rate were manipulated. During several tests, the pressure was also adjusted at the beginning of each run using the hydro-static pump at the bottom of the system. The objective of these tests was to demonstrate natural circulation within the loop.

4.1.1 Atmospheric Pressures

The first test was run at low pressure using various flow rates. The test criteria is listed in Table 4.1.

Table 4.1: Loop test conditions

Loop Test Conditions	Heater Input (W)	Cooling Flow (kg/s)	Initial Pressure, kPa(g)
	2000	0.03 (0.5 gpm)	69 kPa (10 psig)

In the absence of a proper flow meter, circulation can be inferred by observing the system temperatures around the loop. In this system, a stable or reduced temperature at the outlet of the heater despite consistent heat input means that the heat exchanger is effectively removing heat. That means the water is flowing through the tubes of the heat exchanger, facilitating heat transfer.

When the cooling water is turned on, the internal working fluid starts to flow as heat is removed. Figure 4.1 demonstrates this phenomenon. As cooling water is turned on at t = 1 minute, the removal of heat drives the flow rate up and the effectiveness of the heat exchanger increases. This leads to a temperature increase at the heat exchanger hot inlet as heat can be moved more effectively from the lower end of the loop. Once the flow rate reaches steady state, the hot inlet is reduced and the amount of heat removed becomes steady. The steady heat removal starts at 2.5 minutes in Figure 4.1.

The cooling water temperatures, or the heat exchanger cold side temperatures, are shown in Figure 4.2.

The loop's variable mass flow rate prior to steady state can also be observed in the temperature profile at the lower sections of the loop. The temperature measurements above and below the heater, shown in Figure 4.3, show that there is a visible effect on temperatures as the cooling water is turned on at one minute. The rate of heat removal is faster in the earlier time frame, prior to the loop achieving steady

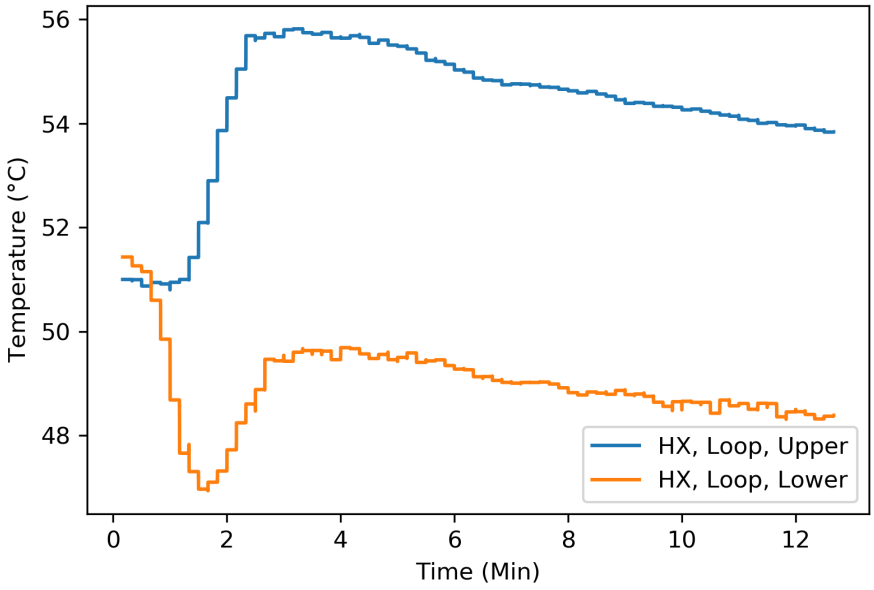

Figure 4.1: Heat exchanger temperatures during low pressure testing. The main loop heater is started initially. At 1 minute, the cooling water is set to a flow rate of 0.03 kg/s (0.3 gpm), starting natural circulation flows.

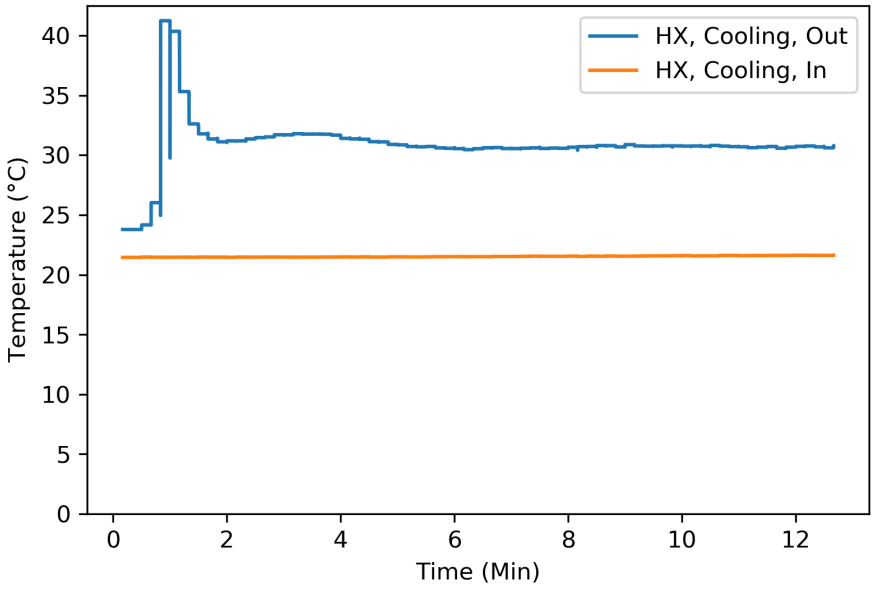

Figure 4.2: Heat exchanger cold side temperatures. Note that the marked decrease at t=1 min was caused by a loose TC connection in the cooling water return reservoir.

state. This follows the phenomenon presented in Figure 4.1.

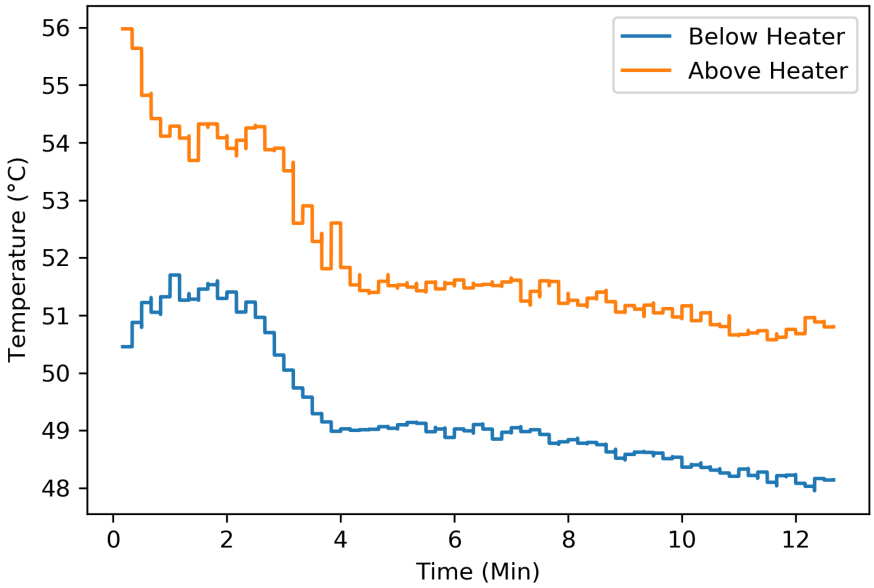

Figure 4.3: Temperature profiles within the loop above and below the heater jacket.

Hot leg temperature is measured by four multipoint thermocouples spaced 48 in apart. The axial temperature profile through the center of the hot leg is plotted in Figure 4.4. The bottom of the hot leg (multipoint 1) is initially at a higher temperature than the top (multipoint 2). As the heater and heat exchanger are engaged, the upper portions of the hot leg reach slightly higher temperatures than the lower portions. This is a good indicator that heat is drawn up and away from the heater via natural circulation flows.

The hot leg instrumentation also gives the ability to investigate the cross sectional temperature profile. Figure 4.5 shows the radial temperature profile at various axial positions up the hot leg pipe section. On plot for each is included for 2 minutes, 6 minutes, 10 minutes, and 14 minutes into the simulation. At 2 minutes, all hot leg temperatures are their respective hottest. As time progresses, the cooling heat exchanger comes to an equilibrium with the heat, reducing the overall temperature in the hot leg. The axial temperature profiles collapse as the system is brought to thermal equilibrium. Radially, each temperature profile is relatively flat with the exception of the measurement on the side of TC insertion. The thermocouples are mounted on alternating sides moving up the hot leg. The dips in temperature at the insertion end show that non-trivial heat loss is occurring at each mounting point.

Figure 4.6 displays the non-dimensionalized temperature profile throughout the loop. From this plot, it can be observed that the rate of temperature change per unit length is roughly equivalent in the heater and heat exchanger sections. This is expected, as they are both about the same length, and the majority of temperature addition or reduction should be occurring in these sections.

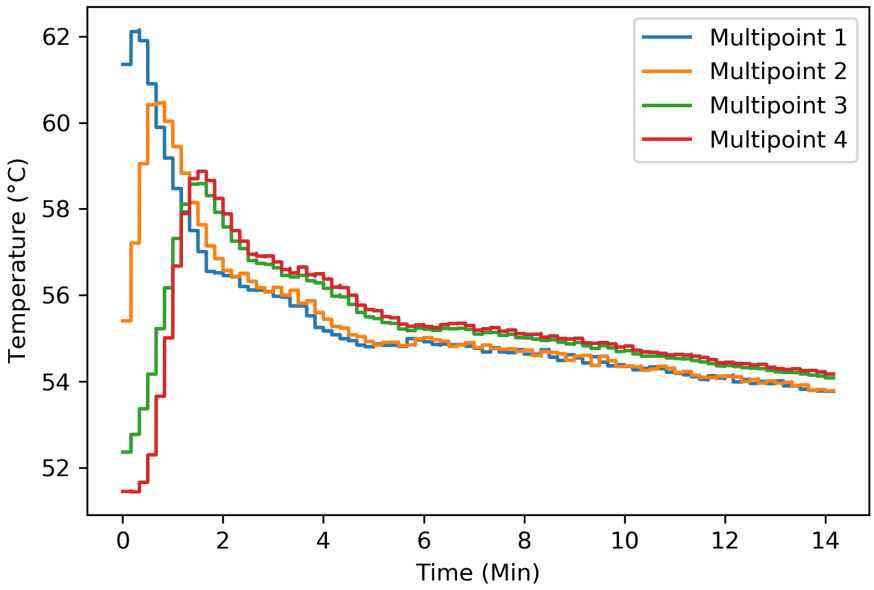

Figure 4.4: Axial temperature profile up the center of the hot leg. Multipoint 1 is the lowest TC and Multipoint 4 is the highest.

4.1.2 Higher Pressures

A preliminary test was run at higher pressures via the hydro-static test pump. The hydro-static pump was used to pressurize the system to an initial pressure of 1723.69 kPa (250 psi). Similar to the low pressure tests, cooling flow rate was set to match heater input. Table 4.2 shows the test conditions for the high pressure test.

Table 4.2: Loop High Pressure Test Conditions

Heater Input (W)	Cooling Flow (kg/s)	Initial Pressure, kPa(g)
2000	0.03 (0.5 gpm)	1723.69 kPa (250 psi)

In the higher pressure test, the transient effect of variable flow rate was less pronounced. Figure 4.7 shows the same increase in loop hot side and decrease loop in cold side before decreasing as it reaches equilibrium. This effect is lessened in the high pressure case, relative to the previous low pressure cases, because the viscosity is higher, meaning the density gradient to drive natural circulation is lower. This scenario, though temperatures are similar to the previous tests, is barely achieving natural circulation throughout the loop.

The cooling, or heat exchanger shell side, water temperatures are displayed in Figure 4.8.

Figure 4.9 shows that the system at heater jacket entrance and exit reached a steady state average temperature of 51.5°C at the entrance (below heater) and 54.5°C at the exit (above heater).

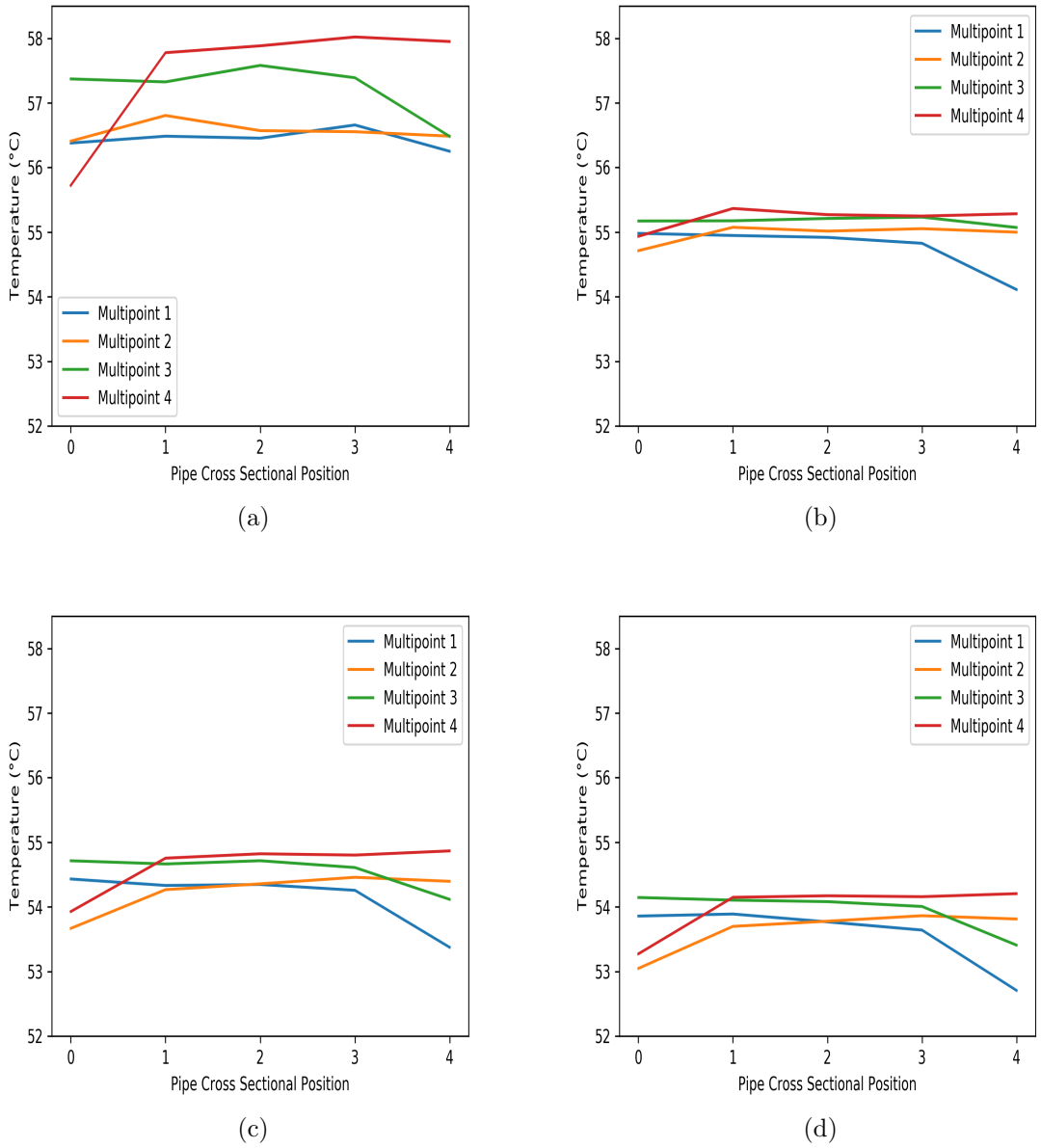

Figure 4.5: Radial temperature profiles of the hot leg at different points in time. The thermocouples are inserted in the hot leg pipe 4 feet from each other, with multipoint 1 being the lowest in elevation and multipoint 4 being the highest. Note that the even numbered TCs are inserted on opposite sides from the odd numbered TCs. a) 2 minutes, b) 6 minutes, c) 10 minutes, d) 14 minutes.

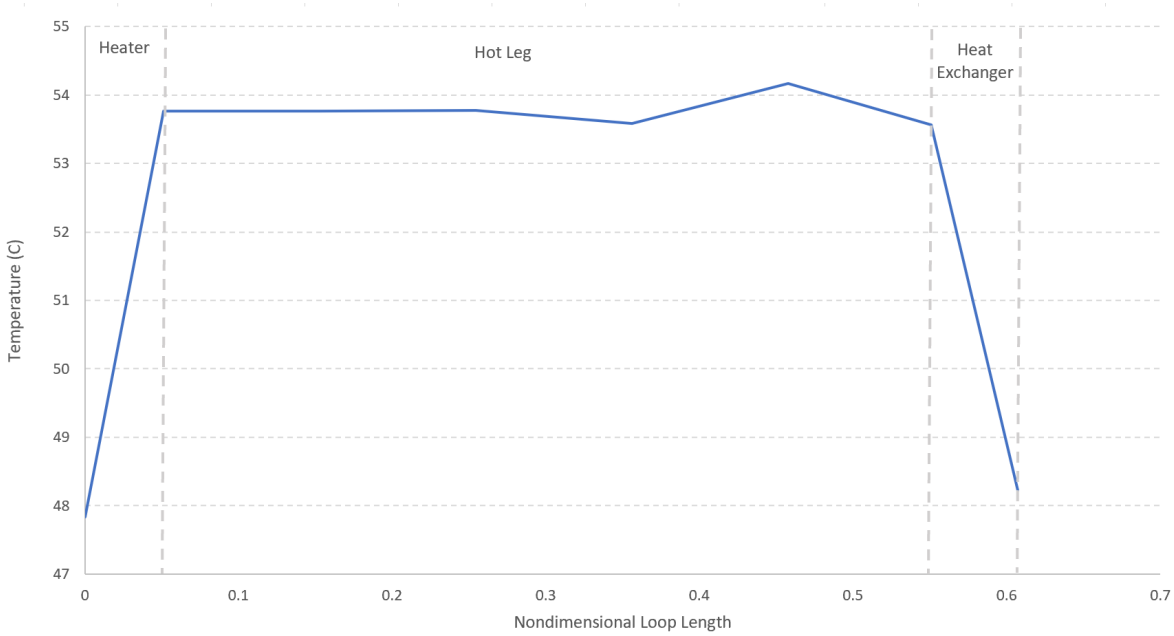

Figure 4.6: Temperature profile plotted against non-dimensionalized length around the loop. 0 and 1 represent the entrance to the heater jacket.

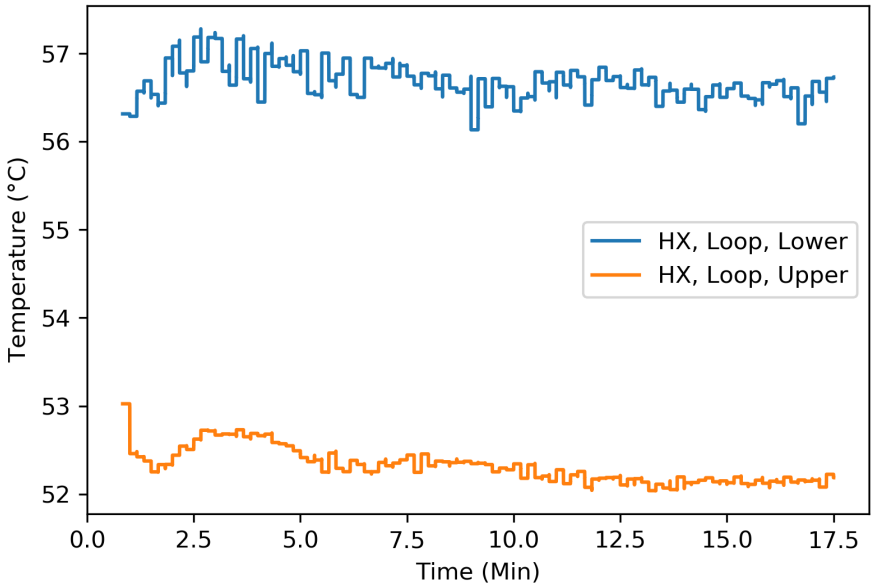

Figure 4.7: Heat exchanger temperatures during high pressure testing. The main loop heater is started initially. The cooling water is set to a flow rate of 0.03 kg/s (0.3 gpm), starting natural circulation flows. Pressure starts at 1723.69 kPa (250 psi).

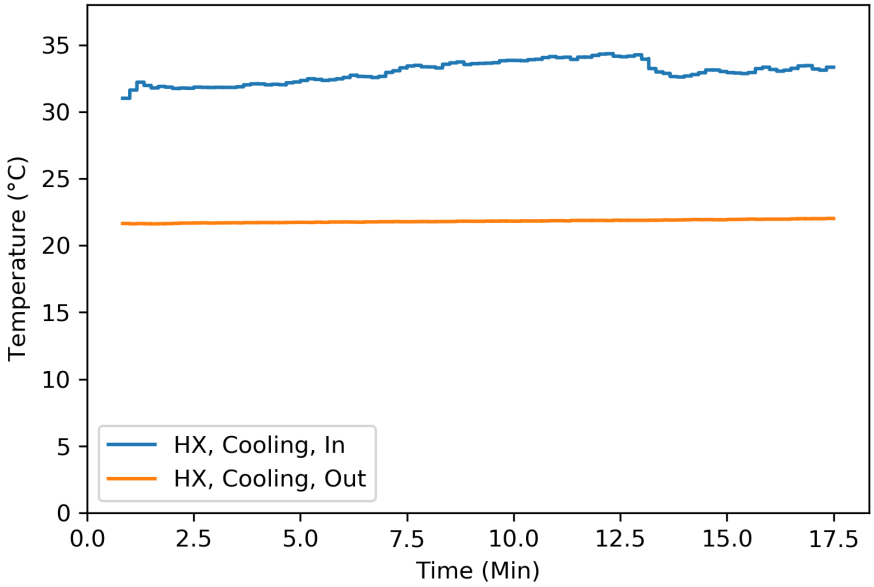

Figure 4.8: Heat exchanger shell side temperatures during high pressure testing.The cooling water is set to a flow rate of 0.03 kg/s (0.3 gpm).

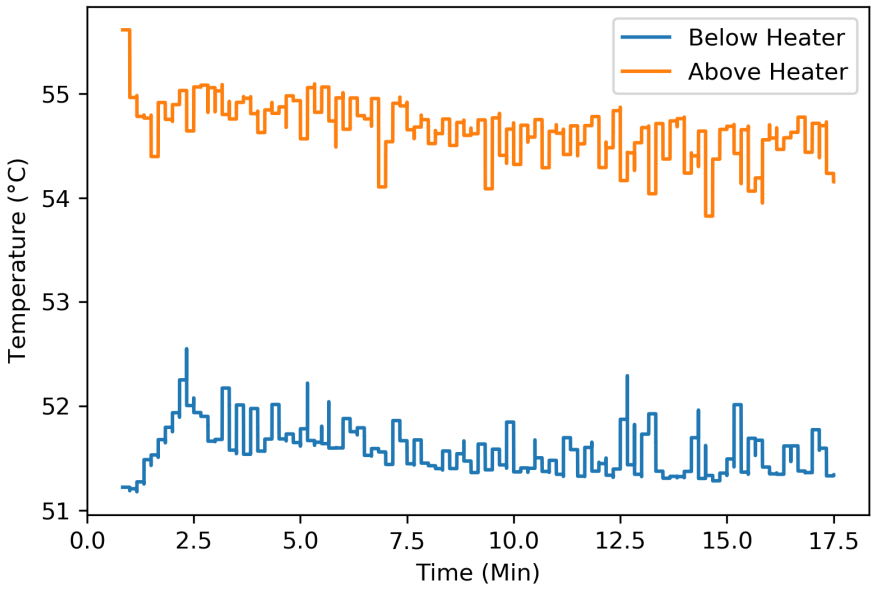

Figure 4.9: Temperature profiles within the loop above and below the heater jacket for higher pressure test.

The data presented from the higher pressure has a high degree of noise. This noise is generally within the 2.2°C error band of the measurement device, but this case should be run again before distinct conclusions can be made on the high pressure case.

4.2 Heat Exchanger Effectiveness

After validating the system flows, heat exchanger effectiveness was evaluated. The cooling water flow rate was varied via the flow meter and gate valve. The cold and hot inlet and outlet temperatures were measured. The experimental data was then used to calculate the heat transferred from hot to cold and the flow rate in the loop. This analysis assumes all the heat from the hot fluid is transferred into the cooling water. The input, measured, and calculated parameters are listed in Table 4.3. Cooling flow rate is input, temperatures in and out of both the cold and hot side of heat exchanger are measured, and heat transferred and loop flow rate are calculated.

Table 4.3: Heat Exchanger Data From Experimental Runs

Cooling Flow (kg/s)	$T_{h,i}$ (C)	$T_{h,o}$ (C)	$T_{c,i}$ (C)	$T_{c,o}$ (C)	Heat (W)	Loop Flow (kg/s)
0.02 (0.3 GPM)	55.0	50.6	21.9	36.0	1110.7	0.06 (0.9 GPM)
0.03 (0.5 GPM)	54.7	48.7	21.9	30.7	1155.4	0.04 (0.7 GPM)
0.04 (0.7 gpm)	55.2	49.4	22.2	31.2	1654.25	0.06 (1.0 GPM)

Using the data in Table 4.3, the heat exchanger effectiveness was calculated. The hot and cold side heat capacity rates were found via average heat capacity from NIST refProp and the corresponding flow rates. The ratio of heat capacity rates was then calculated for each scenario. The cold side flow rates of 0.3, 0.5, and 0.7 corresponded to heat capacity rate ratios of 0.31, 0.64, and 0.68, respectively. The ratios (C_r) are then plugged into Equation 4.1 with NTU varied between 0 and 5 to find effectiveness (ϵ). The curve representing this process is show in Figure 4.10.

$$\epsilon = \frac{1 - exp(-NTU(1 - C_r))}{1 - C_r exp(-NTU(1 - C_r))} \tag{4.1}$$

In addition to heat exchanger effectiveness, the convective heat transfer coefficient was calculated for the hot and cold sides and the overall transfer coefficient (U). Utilizing Newton's Law of Cooling, given in Equation 4.2, the inner and outer convective heat transfer coefficient. A resistive heat transfer network, shown Figure 4.11, was used to calculate the overall heat transfer coefficient.

These heat transfer coefficients generally agree with the NTU calculations and literature convective heat transfer coefficients. The calculated coefficients are tabulated in Table 4.4. The inner and outer heat transfer coefficients were input into Equation 4.2 which yielded NTUs that matched the curves produced in Figure 4.10. The convective heat transfer coefficients also match literature data, with water natural convection schemes usually entering in the 50-3000 W/m^2K range [40].

$$q = hA\Delta t \tag{4.2}$$

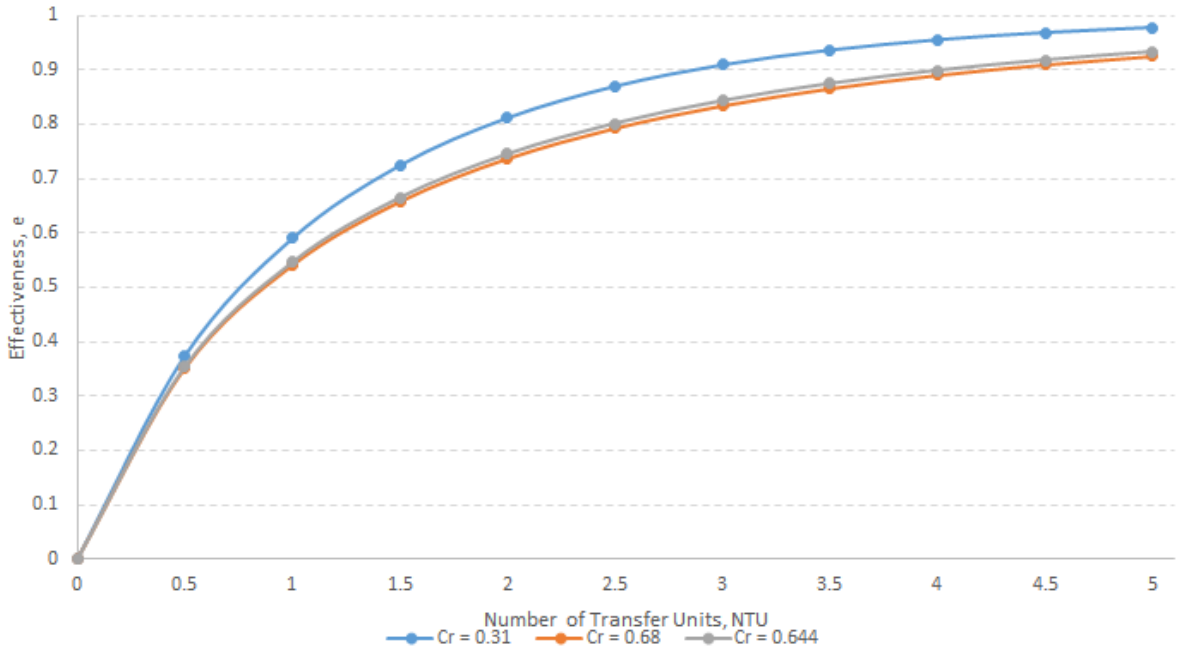

Figure 4.10: NTU effectiveness of loop heat exchanger.

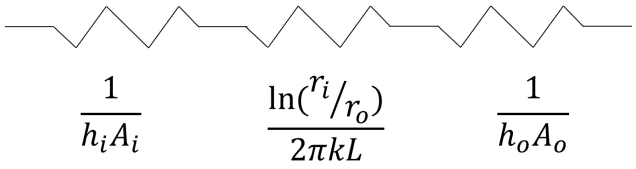

Figure 4.11: Thermal resistance network for calculating overall heat transfer coefficient (U). A represents the heat transfer area, L is length of heat transfer, h is the convective heat transfer coefficient, and subscripts i and o are inner and outer, respectively.

Table 4.4: Convective Heat Transfer Coefficient For Tube (h_i), Shell (h_o), and Overall (U).

Cooling Flow (kg/s)	h_i (W/m^2K)	h_o (W/m^2K)	U (W/m^2K)
0.02 (0.3 GPM)	3277.5	681.8	7.48
0.03 (0.5 GPM)	2500.1	1136.4	9.72
0.04 (0.7 gpm)	3703.2	1591.0	13.9

4.3 Heat Loss and Pressure Drop

The differences in temperatures at the top and bottom of the hot leg can be used to approximate heat losses throughout the system. In an adiabatic system at steady state, the heater exit and the heat exchanger inlet temperatures would be equivalent. In the experimental rig, a system that is at steady state, but not thermal equilibrium, the heat exchanger inlet is actually higher than the heater outlet.

The experimental parameters for calculating heat loss are shown in Table 4.5 for the three low pressure tests at different cooling water flow rates and heat inputs.

Table 4.5: Experimental Parameters for Heat Loss Calculation

Parameter	value
Cold Leg Length	7.0 m
Average ΔT along cold leg	0.95 °C
Loop Flow Rate	0.06 kg/s

The heat loss is calculated by taking the heat input by the heater and subtracting the heat from removed by the heat exchanger. The theoretical difference should be zero because the heater and cooling flow rate were matched to add and remove the same heat. It can be assumed that the difference in heat input and heat removed is lost to the surroundings before it can be removed via heat exchanger.

The heat lost to the surroundings is approximately 477.5 W or 39.8 W/m. This heat loss is higher than expected. One possible explanation would be poorly insulated flanged connections. The flanges, especially the flanges perpendicular to the flow, are acting as large fins, moving heat away from the fluid. Moving forward, a more specialized flange insulation should be used to mitigate the heat losses. Another source of heat loss was the thermocouple insertion points, as seen by the hot leg cross-sectional temperature profile. Insulating these TCs completely would improve retention of heat. Other points of interest could be anywhere the insulation is lacking, such as around pressure transducers, valves, or the pressurizer.

In addition to heat loss, there is a pressure drop associated with this system. From the low pressure tests, the average at the bottom and top PTs are 57.7 kPa (8.4 psi) and 35.0 kPa (5.1 psi), respectively. The bottom transducer is 5.4 m (212 in) below the upper transducer, so a head of 52.1 kPa (7.56 psi) was taken into account. In total, with height accounted for, the pressure drop through the system was 5.5 kPa (0.80 psi).

4.4 Pressurization and Pressurizer Operation

Originally, the pressurizer was developed to control pressure electronically. A heater was sized to add heat to the system and boil water, getting the pressurizer, and the system to the correct saturation temperature.

In practice, the pressurizer had several shortcomings that need to be remedied. The main issue was the time that it took the heater to achieve temperature. With the 800W heater, the pressurizer could not reach the set point of 290 °C. The small heater would dissipate heat through the water in the loop in addition to the pressurizer. The loop water acted as a heat sink, thus making the heater ineffective.

A larger heater would would also decrease the time required to reach system pressure. Additionally, even heating would be useful for the loop as well as the pressurizer, so the case for a pump or other heaters is strong. The Tempco Temperature Controller proved adequate for this system, with the self training PID function working well. The physical design of the pressurizer also met system needs, with a robust container and temperature and pressure measurements.

The pressurizer ought to be able to handle the expansion of water as density decreases. At the original set point, water density decreases to 849 kg/m^3. This equates to all the water in the system expanding an additional 6.6 l. The pressurizer should be able absorb all of this expansion. Thus, the current pressurizer configuration is too small to properly handle insurge events.

In addition to a larger tank, two other changes are proposed for the pressurizer. First, the ability isolate the pressurizer, heat the loop with the large heater separately while the pressurizer comes to temperature, and open the valve when equilibrium is reached. The loop fluid would ingress into the pressurizer, reducing temperature, but then the pressurizer would be better able to restore heat and ultimately boil water, increasing the pressure in the system.

The second change would be to add equipment to heat the entire loop more evenly, either in the form of a pump or strategically placed external heaters. With the system nearing operational conditions, the additional equipment could be turned off and the pressurizer heater used to finish heating the pressurizer to the set point. This would ensure less heat lost from the pressurizer to the rest of the system.

It would also be useful to investigate the pressurizer at the upper end of the system to smooth out fluctuations due to hydraulic head. The ease of changing locations with the heater, TC, and control mechanisms would need to be evaluated against the improved control to make sure moving the pressurizer is worthwhile.

4.5 Computational and Experimental Fluid Dynamics Comparisons

The experimental data from this loop can be compared to the CFD work put forth in the dissertation put forth by Strombach [45]. That study modeled this loop in Ansys Fluent and investigated natural circulation at steady state conditions. A heat of 4000W was applied at the heater and the heat exchanger was used to remove 4000W. The system was assumed to be adiabatic.

The temperature profile from that study is reproduced in Figure 4.12. Though the temperature is lower overall and the heater input is greater, the temperature profile shapes show good agreement. In the CFD analysis, the hot leg temperature profile is relatively flat, similar to experimental data. This system also begins to naturally circulate at a temperature difference of 9°C with a heat input of 4000W. The experimental data shows the loop circulating at 2000W with a temperature difference of 4.5°C. Both of these results seem reasonable in comparison to each other since approximately half the heat input requires half the temperature difference.

Table 4.6 compares the pressure drop from CFD simulations and the experimental data. The relative pressure drop is taken relative to the upper loop pressure. The relative pressure drop in the experimental data is lower than the relative drop in CFD. This is potentially due to a slower velocity in the experimental

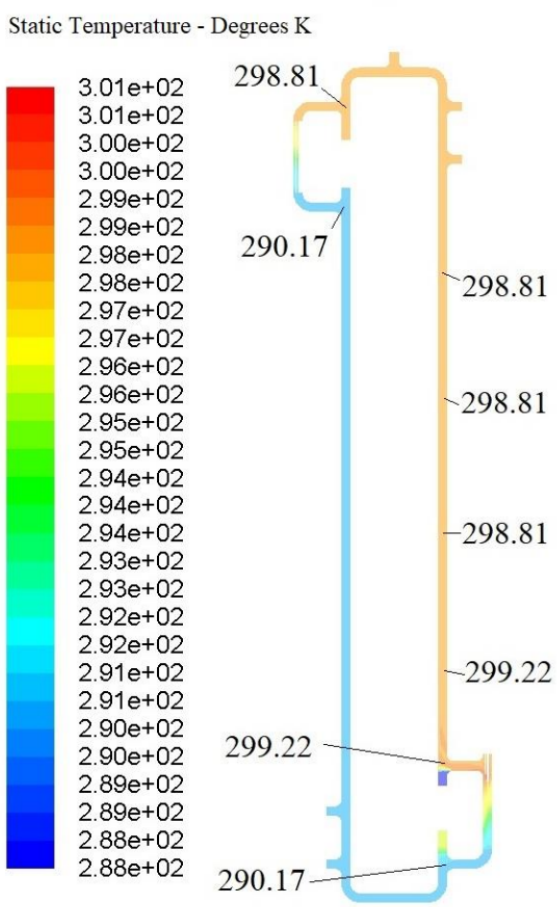

Figure 4.12: CFD analysis of natural convection loop as performed in [45].

data. The CFD runs had an average fluid velocity of 0.0336 m/s while the average velocity in the experimental rig was 0.0000143 m/s. This difference is slightly offset by the experimental tests at a higher temperature and pressure, meaning the viscosity was higher.

Table 4.6: Experimental Pressure Drop Compared to CFD

Region	P_{exp} (Pa)	P_{CFD} (Pa)
Upper Loop	34,955.0	104.0
Lower Loop	5,514.3	6.0
Pressure Drop	29,440.7	98.0
Relative Pressure Drop	84.2%	94.4%

This initial experimental and CFD comparison shows promise for future comparison studies. Running the CFD and the experimental work at exactly the same heat and flow conditions would lead to a more meaningful comparison.

4.6 Applicability of Loop for Modeling Other Fluids

With the data gathered previously and the system geometry, this section puts forth applicable non-dimensional analysis and scaling laws. The purpose of these scaling laws is to compare naturally circulating water in this loop with other working fluids and geometries. The scaling is based on work done by Ishii and Kataoka [46]. Each of the non-dimensional numbers, defined in [46], can be compared between a model and a prototype. The model corresponds to the system that is to be estimated. The prototype corresponds to the known system, in this case the natural circulation loop with water. This analysis assumes a single phase, steady state system. Equations 4.3 - 4.8 show the Richardson number, friction number, modified Stanton number, time ration number, Biot number, and heat source number.

$$R \equiv \frac{g\beta\Delta T_o l_o}{u_o^2} = \frac{buoyancy}{inertia\ force} \tag{4.3}$$

$$F_i \equiv (\frac{fl}{d} + K) = \frac{friction}{inertial\ force} \tag{4.4}$$

$$St_i \equiv \frac{4hl_o}{\rho C_p u_o d} = \frac{wall\ convection}{axial\ convection} \tag{4.5}$$

$$T_i^* \equiv \frac{\alpha_s}{\delta^2}\frac{l_o}{u_o} = \frac{transport\ time}{conduction\ time} \tag{4.6}$$

$$B_i \equiv \frac{h\delta}{k_s} = \frac{wall\ convection}{conduction} \tag{4.7}$$

$$Q_{si} \equiv \frac{q_s l_o}{\rho_s C_{ps} u_o \Delta T_o} = \frac{heat\ source}{axial\ energy\ change} \tag{4.8}$$

Each of the above non-dimensional parameters were calculated for the water system loop and a uranyl-nitrate natural circulation reactor design given in [47]. The comparison of each is given in Table 4.7. The

comparison assumes that stainless steel was used in both systems.

Table 4.7: Comparison of Scaling Parameters Between Natural Convection Loop and Uranyl-Nitrate Reactor

Dimensionless Params	Natural circulation Loop	Uranyl-Nitrate Reactor	Ratio
Richardson	803.7	880.4	1.09
Friction number	24.56	26.71	0.934
Stanton	0.1170	0.0207	0.177
Time number	1.33e09	7.20e08	0.54
Biot	0.0034	0.0040	0.84
Heat source number	0.7955	10.048	0.0095

The Richardson number matches well between both geometries, meaning the flow patterns, or ratio of buoyancy and inertia forces, scale well between the natural convection loop and the reactor design. The non-dimensional friction values are also very similar. In scaling for natural convection, a similar heat source number is important, and but these two systems match poorly. To remedy this, the natural circulation test loop could increase heat input, from 2 kW to 20kW.

In addition to scaling to other systems, the natural circulation loop can be compared to derived literature correlations. A modified Grashof number, according to the methods put forth in [31], was calculated and plotted against literature correlations. Figure 4.13 shows the correlations plotted by Vijayan and Austregesilo with the high and low pressure data points from this work added. The modified Grashof numbers for the two points lies just beyond the limits of the correlations given. Because of the small number of samples, more tests could be done to develop an extension to the correlations given.

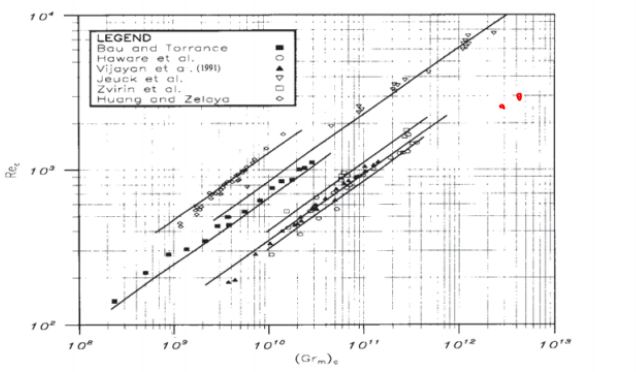

Figure 4.13: Correlations for relating Grashof number to Reynolds number in natural circulation loop scaling. The red data points are the experimental data found in this analysis. Plot from [31].

Chapter 5: Summary and Conclusions

This document puts forth the design, setup, and initial testing of a natural circulation test facility. The loop utilizes an inline heater and a heat exchanger to add and remove heat from the system. The overall system is controlled by heater voltage and cooling water flow rate. A pressurizer was designed to control pressure, with a hydrostatic pump that could be used as a backup to pressurize the system.

The loop displayed characteristics of natural circulation flows. The temperature profiles throughout the system that hot water was moving up from the heater to the heat exchanger. The heat exchanger removed heat to bring the system to a steady state where the heat put in approximately matched the heat removed.

A tube in tube heat exchanger was built for this system. The heat and internal steady state flow rate were calculated. Heat exchanged between the two streams in lower than expects, but the benchmark calculations did not account for any heat losses in the system. Further quantification of the heat losses would be helpful for validation of the heat exchanger. The heat exchanger effectiveness curve was derived and it matches well with the general counter-current tube in tube heat exchanger curve.

Several modeling systems were also used to validate the calculated and experimental data. An Aspen Hysys model was used to validate the initial first principles calculations. The flow rates were found to agree within 2% across the original test horizon.

This experimental work also showed preliminary agreement with CFD simulations. The CFD simulations, though run at a different heat load and a lower temperature, compare favorably. The CFD results with a 4000W heat input have a hot and cold leg temperature difference of 9°C. The experimental loop at 2000W heat input have a hot and cold leg difference of 4.5°C. With half the heat input, half the change in temperature occurs. Further studies with experiments and CFD at the same conditions would offer meaningful comparisons. Modeling natural circulation with CFD is often difficult. The accuracy with which CFD can model these systems is often unknown. This loop can be easily set to a wide variety of temperatures, pressures, and heat inputs to compare with simulations. Doing so would inform the literature on the ability of CFD to model thermosiphons and natural convection phenomena in general.

The experimentation also found that the pressurizer was inadequate for pressurizing this system. The 800W heater was too small and the vessel needs to be larger to correctly handle insurge events. The control system was adequate to adjust the heater based on pressurizer temperature inputs.

5.1 Future Work

This system has shown potential to drive natural circulation and collect meaningful data. Several improvements to the system should be made to increase accuracy and usability.

The first improvement would be additional equipment to help the system reach thermal equilibrium more quickly. The current setup localizes heat at the bottom of the loop and has a difficult time circulating heat throughout the entire system. During 6+ hour run times, the loop's average temperature would only increase about 30°C, while the heater jacket would have localized pockets of high temperatures. This indicates that heat was not being moved effectively around the loop.

Two possibilities for heating the system evenly include adding a pump or adding external heaters in

diverse locations around the system. A pump, used to drive flows while heating the loop initially, would spread the heat from the internal heater more evenly throughout the loop. This would be advantageous because no other heaters would be needed. The difficulty with adding a pump comes in either dealing with the pressure losses of naturally circulating flows moving through an inactive pump, or trying to isolate the pump from the rest of the system when testing natural convection. Isolation could potentially be achieved by the unused, upper accessory flanges, but this would require additional equipment fabrication.

The other option for heating more evenly would be to add external heaters to various sections around the loop. This would distribute heat more evenly and would not require any disturbance in current flow patterns. The drawbacks of this solution is that many individual heaters would more difficult to control and they would require much more input energy.

Another recommendation for improving this system would be to mitigate heat losses. The radial temperature profiles from the hot leg showed that heat was lost at the thermocouple insertion points. Insulating the entire TC and weld-o-let connection would help reduce this. A more effective flange insulation should also be used and the valves on the top and bottom of the system should be insulated. A working pressurizer would also ensure that heat losses along the pressurizer are compensated for via the pressurizer heater.

The cooling water system worked as expected, but could be improved by using a more precise flow meter. Larger cooling reservoirs would also increase the runtime of the system.

In the future, the pressurizer will also need to be revisited. A large fluid volume and a large heater will most likely be needed to achieve pressures suitable for molten salt or sodium surrogate studies. Adding a equipment for more even loop heating would help the pressurizer get to temperature, as less heat would be lost into the surrounding system. It would also be useful to have a way to isolate the pressurizer fluid from the loop fluid during start up so that both parts can reach their appropriate temperatures without as much interference from the other. At that point the fluids could be allowed to mix and the entire system taken to the appropriate conditions.

The pressurizer's current control scheme uses a single input-single output control scheme based on temperature and heat input. For a truly automated system, a level control scheme could be implemented and reduce the need for monitoring. This was originally explored, but level sensors at the desired operating conditions were difficult to find or cost prohibitive. It would be useful to revisit this for improving the pressurizer control.

After the previously mentioned improvements are made, it would be worthwhile to move towards using other fluids in this system. Additional fluids, such as Dowtherm A, could be used a surrogates for different conditions than the water.

References

[1] Yunus A. engel and John M. Cimbala. *Fluid Mechanics: Fundamentals and Applications*. McGraw-Hill Higher Education, 2010.

[2] Technology Overview | NuScale Power.

[3] Hongbin Zhang, Haihua Zhao, Vincent Mousseau, and Ronaldo Szilard. Design Considerations for Economically Competitive Sodium Cooled Fast Reactors. page 13, 2009.

[4] Eugene Engmann, John Peterson, and James Richards. Design of the Molten Salt Nuclear Battery. Washington D, November 2019. American Nuclear Society.

[5] PRISM. Technical report, IAEA.

[6] Anwar Hussain and Amjad Nawaz. The investigation of nonavailability of passive safety systems effects on small break loca sequence in ap1000 using RELAP5 MOD 4.0. *Science and Technology of Nuclear Installations*, January 2016. Publisher: Hindawi Limited.

[7] Ji Xing, Daiyong Song, and Yuxiang Wu. HPR1000: Advanced Pressurized Water Reactor with Active and Passive Safety. *Engineering*, 2(1):79–87, March 2016.

[8] W Brettschuh and D Schneider. Modern light-water reactors - EPR and SWR 1000. Present status and possibilities of development and application.

[9] Ye Bai, Liang Wang, Shuang Zhang, Ningning Xie, and Haisheng Chen. Heat transfer characteristics of a natural circulation separate heat pipe under various operating conditions. *International Journal of Heat and Mass Transfer*, 126:191–200, November 2018. Publisher: Pergamon.

[10] OKLO DG-1353 Pilot. License Application Oklo-2018-RlO-P, Rev. 0, NRC, Washington D.C., September 2018.

[11] Marc A. Gibson, Steven R. Oleson, David I. Poston, and Patrick McClure. NASA's Kilopower reactor development and the path to higher power missions. In *2017 IEEE Aerospace Conference*, pages 1–14, March 2017.

[12] Thermal-FluidsPedia | Fabrication and testing of heat pipes | Thermal-Fluids Central.

[13] Ajay Kumar Yadav, M. Ram Gopal, and Souvik Bhattacharyya. Effect of Tilt Angle on Subcritical/Supercritical Carbon Dioxide-Based Natural Circulation Loop With Isothermal Source and Sink. *JOURNAL OF THERMAL SCIENCE AND ENGINEERING APPLICATIONS*, 8(1, SI), March 2016. Backup Publisher: ISHMT; ASME Place: TWO PARK AVE, NEW YORK, NY 10016-5990 USA Publisher: ASME Type: Article; Proceedings Paper.

[14] Mehmet Esen and Hikmet Esen. Experimental investigation of a two-phase closed thermosyphon solar water heater. *Solar Energy*, 79(5):459–468, November 2005.

[15] L. Luzzi, M. Misale, F. Devia, A. Pini, M. T. Cauzzi, F. Fanale, and A. Cammi. Assessment of analytical and numerical models on experimental data for the study of single-phase natural circulation dynamics in a vertical loop. *Chemical Engineering Science*, 162:262–283, April 2017.

[16] Darius D Lisowski, Mitch T Farmer, S Cass Avenue, and Lemont Il. Experimental Observations of Natural Circulation Flow in the NSTF at Steady-State Conditions. page 7, 2014.

[17] Asghar Alizadehdakhel, Masoud Rahimi, and Ammar Abdulaziz Alsairafi. CFD modeling of flow and heat transfer in a thermosyphon. *International Communications in Heat and Mass Transfer*, 37(3):312–318, March 2010.

[18] Mark Ho, Yeongshin Jeong, Haneol Park, Guan Heng Yeoh, and Weijian Lu. Using CFD as Preventative Maintenance Tool for the Cold Neutron Source Thermosiphon System. *Science and Technology of Nuclear Installations*, 2017, January 2017. Publisher: Hindawi Limited.

[19] Yinfeng Wang, Xiaoyuan Wang, Haijun Chen, Robert Taylor, and Yuezhao Zhu. A combined CFD/visualized investigation of two-phase heat and mass transfer inside a horizontal loop thermosiphon. *International Journal of Heat and Mass Transfer*, 112:607–619, September 2017. Publisher: Pergamon.

[20] Mayurkumar Ghandi, Mayur Sathe, Jyeshtharaj Joshi, and Pallippattu Vijayan. Two phase natural convection: CFD simulations and PIV measurement. *Chemical Engineering Science*, 66(14):3152–3171, July 2011. Publisher: Pergamon.

[21] Mayurkumar Ghandi, Jyeshtharaj Joshi, and Pallippattu Vijayan. Study of two phase thermal stratification in cylindrical vessels: CFD simulations and PIV measurements. *Chemical Engineering Science*, 98:125–151, July 2013. Publisher: Pergamon.

[22] Eshita Pal, Mukesh Kumar, Arun K. Nayak, and Jyeshtharaj B. Joshi. Experimental and CFD simulations of fluid flow and temperature distribution in a natural circulation driven Passive Moderator Cooling System of an advanced nuclear reactor. *Chemical Engineering Science*, 155:45 – 64, 2016.

[23] David Pialla, Denis Tenchine, Simon Li, Paul Gauthe, Alfredo Vasile, Roland Baviere, Nicolas Tauveron, Fabien Perdu, Ludovic Maas, Franois Cocheme, Klaus Huber, and Xu Cheng. Overview of the system alone and system/CFD coupled calculations of the PHENIX Natural Circulation Test within the THINS project. *Nuclear Engineering and Design*, 290:78–86, August 2015.

[24] Afshin Hedayat. Simulation and transient analyses of a complete passive heat removal system in a downward cooling pool-type material testing reactor against a complete station blackout and long-term natural convection mode using the RELAP5/3.2 code. *Nuclear Engineering and Technology*, 49(5):953–967, August 2017.

[25] Patrick Freitag. *Transient Thermal Hydraulic Simuation of a Small Modular Reactor in RELAP 5*. PhD thesis, University of Rhode Island, Providence, RI, 2018. Library Catalog: ida.lib.uidaho.edu:2096.

[26] C.M. Allison and J.K. Hohorst. Role of RELAP/SCDAPSIM in Nuclear Safety - ProQuest. *Science and Technology of Nuclear Installations*, 2010, 2010. Library Catalog: ida.lib.uidaho.edu:2096.

[27] Sadaf Zaidai. Development of support vector regression (SVR)-based model for prediction of circulation rate in a vertical tube thermosiphon reboiler. *Chemical Engineering Science*, 69(1):514–521, February 2012. Publisher: Pergamon.

[28] Z. J. Zuo and F. S. Gunnerson. Numerical modeling of the steady-state two-phase closed thermosyphon. *International Journal of Heat and Mass Transfer*, 37(17):2715–2722, November 1994.

[29] Jianfeng Xu. *Theoretical and experimental analysis of two-phase closed thermosyphons.* PhD thesis, University of Alaska Fairbanks, Fairbanks, AK, May 2008. Library Catalog: ida.lib.uidaho.edu:2096.

[30] Haojie Cheng, Haiyan Lei, and Chuanshan Dai. Heat Transfer of a Single-Phase Natural Circulation Loop With Heating and Cooling Fluids. *Energy Procedia*, 142:3926–3931, December 2017.

[31] P. K Vijayan and H Austregesilo. Scaling laws for single-phase natural circulation loops. *Nuclear Engineering and Design*, 152(1):331–347, November 1994.

[32] Dipankar N. Basu, Souvik Bhattacharyya, and P.K. Das. Development of a unified model for the steady-state operation of single-phase natural circulation loops. *International Journal of Heat and Mass Transfer*, 62:452 – 462, 2013.

[33] Yukyung Shin, Seok Bin Seo, In Guk Kim, and In Cheol Bang. Natural circulation with dowtherm rp and its mars code implementation for molten salt-cooled reactors. *International Journal of Energy Research*, 40(8):1122–1133, 2016.

[34] Kazuhiro Oyama, Junji Endo, Norihiro Doda, Ayako Ono, Takahiro Murakami, and Osamu Watanabe. Development of natural circulation analysis methods for a sodium cooled fast reactor. *JOURNAL OF NUCLEAR SCIENCE AND TECHNOLOGY*, 53(3):353–370, 2016.

[35] Min Ho Lee, Dong Wook Jerng, and In Cheol Bang. Experimental validation of simulating natural circulation of liquid metal using water. *Nuclear Engineering and Technology*, March 2020.

[36] Theodore L. Bergman, Frank P. Incropera, David P. DeWitt, and Adrienne S. Lavine. *Fundamentals of Heat and Mass Transfer.* John Wiley & Sons, April 2011. Google-Books-ID: vvyIoXEywMoC.

[37] Design Institute for Physical Property Data (U.S.), American Institute of Chemical Engineers, and National Institute of Standards and Technology (U.S.). *DIPPR chemical database.* BYU DIPPR, Thermophysical Properties Laboratory, Provo, UT, 1998. OCLC: 43246668.

[38] Finite Element Analysis Software | Autodesk.

[39] Warren Clarence Young, Richard Gordon Budynas, and Raymond Jefferson Roark. *Roark's Formulas for Stress and Strain.* McGraw-Hill, 2002. Google-Books-ID: N_wcQAAACAAJ.

[40] Frank Incropera and David DeWitt. Free Convection. In *Fundamentals of Heat and Mass Transfer*, pages 533–592. John Wiley & Sons, Hoboken, NJ, 5th edition, 2002.

[41] E. W. Lemmon, I.H. Bell, M. L. Huber, and M. O. McLinden. NIST Standard Reference Database 23: Reference Fluid Thermodynamic and Transport Properties-REFPROP, Version 10.0, National Institute of Standards and Technology, 2018.

[42] Aspen Tech. Aspen HYSYS, 2019.

[43] William D. Callister Jr and David G. Rethwisch. *Fundamentals of Materials Science and Engineering: An Integrated Approach.* John Wiley & Sons, 2012.

[44] ITS-90 Thermocouple Database - Introduction.

[45] G. M. Strombach. *Computational Modeling of Flow in a 10MWe Natural Convection Molten Salt Reactor.* PhD thesis, University of Idaho, Moscow,ID, 2020.

[46] M Ishii. Scaling Laws for Thermal Hydraulic System Under Single Phase and Two-Phase Natural Circulation. *Nuclear Engineering and Design*, 81:411–425, 1984.

[47] Teyen Widdicombe, Olin Calvin, Nephi Kharadia, Emmett Armour, Joseph Hafen, Robin Roper, Alberto Cardenas-Melgar, Kevin Terrill, and Joshua Young. Design of a uranyl nitrate natural circulation micro-reactor for medical isotope production. Technical report, University of Idaho, Idaho Falls, ID, May 2020.